CHALMERS

*PREPRINT 2000–005*

# Least-Squares Finite Element Methods for Electromagnetic Applications

Rickard Bergström

*Chalmers Finite Element Center*
CHALMERS UNIVERSITY OF TECHNOLOGY
Göteborg Sweden 2000

Preprint Chalmers Finite Element Center

# Least-Squares Finite Element Methods for Electromagnetic Applications

Rickard Bergström

CHALMERS

Chalmers Finite Element Center
Chalmers University of Technology
SE-412 96 Göteborg, Sweden
Göteborg, May 2000

Least-Squares Finite Element Methods for Electromagnetic Applications
Rickard Bergström
NO 2000–005
ISSN 1404–4382

Chalmers Finite Element Center
Chalmers University of Technology
SE-412 96 Göteborg
Sweden
Telephone: +46 (0)31 772 1000
Fax: +46 (0)31 772 3595
www.phi.chalmers.se

Printed in Sweden
Chalmers University of Technology
Göteborg, Sweden 2000

## Abstract

We investigate the application of LSFEM (least-squares finite element method) to static and time harmonic Maxwell's equations in three space dimensions in cases of industrial significance. We find that with suitable residual weighting and mesh adaptivity, LSFEM gives satisfactory results for problems with discontinuous magnetic permeabilities of largely different orders of magnitude, but without strong corner singularities. We also discuss possible remedies to the indicated basic short-coming resulting from the strong norm residual control in LSFEM.

## Acknowledgements

First of all, I would like to thank my advisors, Professor Claes Johnson, Mats G. Larson, and Mårten Levenstam, for their time, their encouragement, and the many discussions we have had. I also want to thank Klas Samuelsson for helping me with C++ matters.

Furthermore, I am grateful to Arne Wolfbrandts group at ABB, in particular Leif Sehlström, for helping me with test cases and reference solutions.

This work was financially supported by the Foundation for Strategic Research (SSF) through the NTM and NGSSC programs.

Finally, a grateful thought to my grandfather for the inspiration.

# Contents

# Chapter 1

# Introduction

Maxwell's equations describe electromagnetic phenomena in the whole frequency range, from high frequency microwaves used in, e.g., mobile communication, to low frequencies occuring in power engineering. The equations constitute a first order system of eight equations in two unknown vector fields with altogether six components, and thus is an overdetermined system.

The system was stated in complete form by James Clerk Maxwell in the end of the 19:th century. Maxwell was able to find particular wave-like solutions and in this way predicted the possibility of electromagnetic wave propagation before this phenomenon had been observed experimentally; a spectacular success of mathematical science.

The purpose of this thesis is to study the applicability of least-squares finite element methods for the numerical solution of static and time harmonic Maxwell's equations. The work is part of a larger project in cooperation with ABB, aiming at developing and implementing adaptive finite element methods for the full time dependent Maxwell's equations for industrial applications with realistic three dimensional geometry and material data.

The following basic largely open problems are adressed in this project:

- the overspecification in Maxwell's equations,
- solution singularities at interfaces and corners,
- choice of variables (fields or potentials, or combinations thereof),
- choice of finite element discretization (Galerkin, Least-Squares, edge elements, etc.),
- adaptive error control,
- high performance computing (algebraic solvers, parallelization).

## 1.1 Least-Squares Finite Element Methods for Maxwell's Equations

In a least-squares finite element method (LSFEM) a sum of suitable residual norms is minimized over a piecewise polynomial space. The residuals may contain differential equations, constitutive equations, interface and boundary conditions.

LSFEM is a general method with the following features, see, e.g., Bochev and Gunzberger [8], Jiang [18], and [1],

- applicability to general, possibly overspecified, first order systems,
- stability follows directly from well posedness of the continuous problem,
- essential boundary conditions may be imposed weakly, and
- the resulting discrete system of equations is symmetric positive definite.

In particular, LSFEM is applicable to Maxwell's equations in first order form. With the divergence equations included, LSFEM does not suffer from the spurious solutions which may occur in certain Galerkin methods, see, e.g., Jiang, Wu, and Povinelli [19] and the book by Jiang [18].

The strong norm residual minimization of LSFEM in its standard form, makes computation of singular solutions difficult. Another difficulty concerns the weighting of the different residuals. In this thesis, we adress these problems, with focus on static and time harmonic problems.

## 1.2 Some Alternative Approaches

In low frequency electromagnetic problems, a standard approach is to formulate the problem in potentials rather than in the primary field variables. Depending on the problem, one has a range of formulations to use. In the general case, the fields are expressed using one vector and one scalar potential. In order to reduce the number of unknowns and increase the efficiency in the computation, one may in certain regions use only one of these potentials, see, e.g., Touma Holmberg [28].

The potential formulations have the advantage that the sought solution is continuous, in contrast to when seeking a solution in the field variables. Furthermore, the singularities in the primary fields now arise in the derivatives instead. This leads to a more regular solution and discontinuities in material coefficients need no special treatment.

However, the potentials are not necessarily uniquely determined. Then, one has to introduce a suitable gauge condition, alternatively solve an indefinite matrix problem.

The Galerkin finite element method may be applied to the time dependent or time harmonic Maxwell's equations. Spurious solutions may occur in certain situations. This may be overcome by special treatment of the divergence equations as in Assous, Degound, Heintze, Raviart, and Segre [3], or the use of special elements, such as edge elements.

## 1.3 Notation

We let $\Omega$ denote an open bounded domain in $\mathbf{R}^3$, with boundary $\Gamma = \Gamma_1 \cup \Gamma_2$. The standard notation and definition for the Sobolev spaces $H^s(\Omega)$ and $H^s(\Gamma)$, for $s \geq 0$, is used together with the corresponding inner products $(\cdot,\cdot)_{s,\Omega}$ and $(\cdot,\cdot)_{s,\Gamma}$ and norms $\|\cdot\|_{s,\Omega}$ and $\|\cdot\|_{s,\Gamma}$, where in general the index $\Omega$ will be left out. In the special case of $L^2$, the simpler notation $(\cdot,\cdot)$ and $(\cdot,\cdot)_\Gamma$ will be used. For details on the definition of the corresponding dual spaces, when $s < 0$, see, e.g., Evans [14]. We will also make use of the semi-norms

$$|u|_k = \left( \sum_{|\alpha|=k} \|D^\alpha u\|^2 \right)^{1/2}, \tag{1.1}$$

where

$$D^\alpha u = \frac{\partial^{|\alpha|} u}{\partial x_1^{\alpha_1} \partial x_2^{\alpha_2} \partial x_3^{\alpha_3}}, \tag{1.2}$$

$$|\alpha| = \alpha_1 + \alpha_2 + \alpha_3. \tag{1.3}$$

Weighted $L^2$ norms are defined by

$$\|v\|^2_{\Omega,\omega} = \int_\Omega v^2 \omega d\Omega.$$

Since we are dealing with vector fields, we introduce the product spaces $H^{s_1}(\Omega) \times \cdots \times H^{s_n}(\Omega)$. When all the indices $s_i$ are the same, the product space will be denoted by $[H^s(\Omega)]^n$, with the same notation for inner products and norms as above. Another space that occur in this context is

$$H_{div}(\Omega) = \{u \in [L^2(\Omega)]^3 : \nabla \cdot u \in L^2(\Omega)\}, \tag{1.4}$$

with norm defined by

$$\|v\|^2_{H_{div}} = \|v\|^2 + \|\nabla \cdot v\|^2. \tag{1.5}$$

# Chapter 2

# Maxwell's Equations

## 2.1 The Full Equations

Maxwell's equations governing all macroscopic electromagnetic phenomena take the form of the following first order system of partial differential equations:

$$\nabla \times E = -\frac{\partial B}{\partial t}, \tag{2.1a}$$

$$\nabla \times H = J + \frac{\partial D}{\partial t}, \tag{2.1b}$$

$$\nabla \cdot D = \rho, \tag{2.1c}$$

$$\nabla \cdot B = 0, \tag{2.1d}$$

in a domian $\Omega$ in $\mathbf{R}^3$. $E$ and $H$ are the electric and magnetic field intensities respectively, and $D$ and $B$ are the corresponding flux densities, $J = J_{sc} + \sigma E$ is the total current density, $J_{sc}$ is an imposed current density, $\sigma$ is the electric conductivity, and $\rho$ is the charge density.

The electric and magnetic fields are connected to the corresponding fluxes through the following constitutive relations

$$B = \mu H, \tag{2.2a}$$

$$D = \epsilon E, \tag{2.2b}$$

where $\mu$ is the magnetic permeability and $\epsilon$ is the electric permittivity. In the general case of anisotropic media, these parameters are tensors and can be functions of both space and time. They may also depend on the magnetic and electric fields and fluxes, and in lossy media they are complex-valued. In this work, we will only consider the simpler case of linear, homogeneous and isotropic media, where $\epsilon$ and $\mu$ are piecewise constant real scalars. Often, one expresses these parameters as $\epsilon = \epsilon_r\, \epsilon_0$ and $\mu = \mu_r\, \mu_0$, where the index $r$ refers to a relative value and the index 0 is the value in free space, $\mu_0 = 4\pi \times 10^{-7}$ H/m and $\epsilon_0 = \frac{1}{c^2 \mu_0}$ F/m, where $c$ is the speed of light.

Solutions to (2.1) satisfy the following continuity conditions at interfaces:

$$[E] \times n = 0, \tag{2.3a}$$
$$[H] \times n = 0, \tag{2.3b}$$
$$[D] \cdot n = 0, \tag{2.3c}$$
$$[B] \cdot n = 0, \tag{2.3d}$$

where $[\cdot]$ denotes the jump across the interface, and $n$ is a unit normal to the surface, stating that the tangential components of $E$ and $H$ are continuous as well as the normal components of $D$ and $B$. These conditions imply that since $B = \mu H$, the normal component $H \cdot n$ will be discontinuous across an interface of discontinuity of $\mu$. Corresponding relations hold for the other fields. One further observation is that in corners and on edges, where the normal vector abruptly changes direction, these conditions are not consistent leading to a singularity in the solution, see Costabel and Dauge [11] and Assous, Ciarlet and Sonnendrücker [2].

In the special case of a perfect conductor or a perfect magnetic wall, which cannot sustain fields, the interface conditions reduce to

$$E \times n = 0, \tag{2.4a}$$
$$B \cdot n = 0, \tag{2.4b}$$

and

$$H \times n = 0, \tag{2.5a}$$
$$D \cdot n = 0, \tag{2.5b}$$

respectively.

## 2.2 The Quasi-Static Approximation

In many low frequency application, including power engineering, we may set $\epsilon = 0$, and thus $D \equiv 0$, which leads to the following, so called quasi-static form of Maxwell's equations:

$$\nabla \times E = -\frac{\partial B}{\partial t}, \tag{2.6a}$$
$$\nabla \times H = J, \tag{2.6b}$$
$$\nabla \cdot B = 0, \tag{2.6c}$$

where as before, $J = J_{sc} + \sigma E$ and $B = \mu H$. The interface conditions (2.3) reduce to

$$[E] \times n = 0, \tag{2.7a}$$
$$[H] \times n = 0, \tag{2.7b}$$
$$[B] \cdot n = 0. \tag{2.7c}$$

However, since by (2.6b) $\nabla \cdot J = 0$, we have the additional interface condition,

$$[J] \cdot n = 0. \tag{2.8}$$

### 2.2.1 The Time Harmonic Equations

Assuming time dependence of the form $e^{j\omega t}$, we obtain the following time harmonic analog to (2.6):

$$\nabla \times E = -j\omega B, \tag{2.9a}$$
$$\nabla \times H = J, \tag{2.9b}$$
$$\nabla \cdot B = 0. \tag{2.9c}$$

In this case, we work with complex-valued fields even in lossless media.

## 2.3 The Static Equations

In the static case, with no time variation, the equations decouple into an electrostatic system

$$\nabla \times E = 0, \tag{2.10a}$$
$$\nabla \cdot D = \rho, \tag{2.10b}$$

and a magnetostatic system

$$\nabla \times H = J, \tag{2.11a}$$
$$\nabla \cdot B = 0. \tag{2.11b}$$

Of these two, we have only considered the magnetostatic problem, as this serves as a special case of the quasi-static applications. It includes the complication of magnetic materials, leading to discontinuities and singularities in the field variables.

## 2.4 The Div-Curl System

### 2.4.1 Basic Equations

In the case of constant constitutive material parameters, both the magnetostatic and electrostatic systems (2.11) and (2.10) take the form of the following div-curl system: find $u \in [H^1(\Omega)]^3$ such that

$$\nabla \times u = \omega \quad \text{in } \Omega, \tag{2.12a}$$
$$\nabla \cdot u = \rho \quad \text{in } \Omega, \tag{2.12b}$$
$$n \cdot u = 0 \quad \text{on } \Gamma_1, \tag{2.12c}$$
$$n \times u = 0 \quad \text{on } \Gamma_2, \tag{2.12d}$$

where $\omega \in [L^2(\Omega)]^3$ and $\rho \in L^2(\Omega)$ are given data and $\Gamma = \Gamma_1 \cup \Gamma_2$ is the boundary of $\Omega$, where either $\Gamma_1$ or $\Gamma_2$ may be empty. This is a system of four equations in three unknowns and solvability requires the satisfaction of the following compatibility conditions

$$\nabla \cdot \omega = 0 \quad \text{in } \Omega, \tag{2.13a}$$
$$\int_\Gamma n \cdot \omega \, d\Gamma = 0, \tag{2.13b}$$
$$n \cdot \omega = 0 \quad \text{on } \Gamma_2, \tag{2.13c}$$

and, if $\Gamma_2 = \emptyset$,

$$\int_\Omega \rho \, d\Omega = 0. \tag{2.14}$$

Uniqueness of a solution to the div-curl system follows directly from the following result.

**Theorem 2.4.1** *Let $\Omega \subset \mathbf{R}^3$ be a bounded and simply connected domain with a sufficiently smooth boundary $\Gamma = \Gamma_1 \cup \Gamma_2$. If $u \in [H^1(\Omega)]^3$ satisfies*

$$\nabla \times u = 0 \quad \textit{in } \Omega, \tag{2.15a}$$
$$\nabla \cdot u = 0 \quad \textit{in } \Omega, \tag{2.15b}$$
$$n \cdot u = 0 \quad \textit{on } \Gamma_1, \tag{2.15c}$$
$$n \times u = 0 \quad \textit{on } \Gamma_2, \tag{2.15d}$$

*then*

$$u \equiv 0 \quad \textit{in } \Omega. \tag{2.16}$$

**Proof.** Since $\Omega$ is simply connected and $\nabla \times u = 0$, we can introduce a potential $\phi$ such that $u = \nabla\phi$. Then $\phi$ satisfies

$$\Delta\phi = 0 \quad \text{in } \Omega, \tag{2.17a}$$
$$n \cdot \nabla\phi = 0 \quad \text{on } \Gamma_1, \tag{2.17b}$$
$$n \times \nabla\phi = 0 \quad \text{on } \Gamma_2, \tag{2.17c}$$

hence $\phi$ is constant and $u = \nabla\phi \equiv 0$. $\square$

The existence of a solution is proved in Girault and Raviart [15]. Below we will use the following estimate to prove a basic a priori error estimate for the least-squares finite element method.

**Lemma 2.4.2 (The Friedrichs First Div-Curl Inequality)** *Let $\Omega \subset \mathbf{R}^3$ be a bounded and simply connected domain with a sufficiently smooth boundary $\Gamma = \Gamma_1 \cup \Gamma_2$. Then there is a constant $C$, which depends only on $\Omega$, such that*

$$\|u\|_1^2 \leq C\Big(\|\nabla \cdot u\|^2 + \|\nabla \times u\|^2\Big), \tag{2.18}$$

*for every $u \in [H^1(\Omega)]^3$ with $n \cdot u = 0$ on $\Gamma_1$ and $n \times u = 0$ on $\Gamma_2$.*

### 2.4.2 The Elliptic Extension

An alternative approach to the analysis of the div-curl system is to add a "slack" variable and thus obtain a system with four equations in four unknowns which turns out to be elliptic and thus well posed. The slack variable will be zero if the compatibility conditions (2.13) and (2.14) are satisfied.

We thus write the div-curl system (2.12) as

$$\nabla \times u + \nabla\phi = \omega \quad \text{in } \Omega, \tag{2.19a}$$
$$\nabla \cdot u = \rho \quad \text{in } \Omega, \tag{2.19b}$$
$$n \cdot u = 0 \quad \text{on } \Gamma_1, \tag{2.19c}$$
$$\phi = 0 \quad \text{on } \Gamma_1, \tag{2.19d}$$
$$n \times u = 0 \quad \text{on } \Gamma_2, \tag{2.19e}$$

where $\phi$ is the slack variable.

To verify the ellipticity of this system, we write the differential operator on the form

$$\mathcal{L}\sigma = \sum_{i=1}^{3} A_i \frac{\partial\sigma}{\partial x_i} + A_0\sigma, \tag{2.20}$$

where

$$A_1 = \begin{pmatrix} 0 & 0 & 0 & 1 \\ 0 & 0 & -1 & 0 \\ 0 & 1 & 0 & 0 \\ 1 & 0 & 0 & 0 \end{pmatrix}, \quad A_2 = \begin{pmatrix} 0 & 0 & 1 & 0 \\ 0 & 0 & 0 & 1 \\ -1 & 0 & 0 & 0 \\ 0 & 1 & 0 & 0 \end{pmatrix},$$
$$A_3 = \begin{pmatrix} 0 & -1 & 0 & 0 \\ 1 & 0 & 0 & 0 \\ 0 & 0 & 0 & 1 \\ 0 & 0 & 1 & 0 \end{pmatrix}, \quad A_0 = \begin{pmatrix} 0 & 0 & 0 & 0 \\ 0 & 0 & 0 & 0 \\ 0 & 0 & 0 & 0 \\ 0 & 0 & 0 & 0 \end{pmatrix},$$

and

$$\sigma = \begin{pmatrix} u_1 \\ u_2 \\ u_3 \\ \phi \end{pmatrix}.$$

The characteristic polynomial associated with (2.20) is

$$\det(A_1\xi + A_2\eta + A_3\zeta) = (\xi^2 + \eta^2 + \zeta^2)^2 > 0, \tag{2.21}$$

for all nonzero real triplets $(\xi, \eta, \zeta)$, which proves ellipticity.

To see that $\phi$ is zero when the compatibility conditions are satisfied, we make use of Theorem 2.4.1 to derive the following system equivalent to (2.19a):

$$\begin{aligned} \nabla \times (\nabla \times u + \nabla\phi - \omega) &= 0 \quad \text{in } \Omega, && (2.22a)\\ \nabla \cdot (\nabla \times u + \nabla\phi - \omega) &= 0 \quad \text{in } \Omega, && (2.22b)\\ n \times (\nabla \times u + \nabla\phi - \omega) &= 0 \quad \text{on } \Gamma_1, && (2.22c)\\ n \cdot (\nabla \times u + \nabla\phi - \omega) &= 0 \quad \text{on } \Gamma_2. && (2.22d) \end{aligned}$$

Using Lemma 2.4.3 below, we conclude that $\phi$ must satisfy,

$$\begin{aligned} \Delta\phi &= 0 \quad \text{in } \Omega, && (2.23a)\\ \phi &= 0 \quad \text{on } \Gamma_1, && (2.23b)\\ n \cdot \nabla\phi &= 0 \quad \text{on } \Gamma_2, && (2.23c) \end{aligned}$$

which proves that $\phi \equiv 0$ in $\Omega$.

**Lemma 2.4.3** *If $u \in [H^1(\Omega)]^3$ with $n \times u = 0$ on $\Gamma_2 \neq \emptyset$, then $n \cdot \nabla \times u = 0$ on $\Gamma_2$*

**Proof.** We will prove this by contradiction. Assume that $n \cdot \nabla \times u > 0$ at a point $P$ on $\Gamma_2$. Then for some $\epsilon > 0$,

$$n \cdot \nabla \times u \geq \epsilon > 0, \tag{2.24}$$

in a neighborhood $\gamma \subset \Gamma_2$ of $P$ with boundary $\partial\gamma$. By Stokes theorem we get a contradiction

$$0 = \oint_{\partial\gamma} u \cdot ds = \int_{\gamma} n \cdot \nabla \times u \, d\gamma > 0. \tag{2.25}$$

□

# Chapter 3

# The Least-Squares Finite Element Method

## 3.1 General Theory

In this chapter we present the least-squares finite element method for a general first order system, prove basic error estimates assuming well posedness, and give applications to scalar convection, the Poisson equation written as a first order system, and to the main problem of interest: magnetostatics with discontinuous material coefficients.

### 3.1.1 A General First Order Problem

Consider the following first order boundary value problem:

$$\mathcal{L}u = f \quad \text{in } \Omega, \tag{3.1a}$$

$$\mathcal{B}u = g \quad \text{on } \Gamma, \tag{3.1b}$$

where $\Omega$ is a bounded domain in $\mathbf{R}^3$ with boundary $\Gamma$. Here $u$ is a vector of $m$ unknowns and $\mathcal{L}$ is a linear differential operator of the form

$$\mathcal{L}u = \sum_{i=1}^{3} A_i \frac{\partial u}{\partial x_i} + A_0 u, \tag{3.2}$$

and $\mathcal{B}$ is an algebraic boundary operator of the form

$$\mathcal{B}u = Bu, \tag{3.3}$$

where $A_i$ and $B$ are matrices with variable coefficients of type $m \times m$ and $n \times m$ respectively, where $n < m$. These coefficient matrices are assumed to be bounded.

Furthermore, we assume that problem (3.1) has a unique solution, $u$.

### 3.1.2 The Least-Squares Formulation

Now, suppose $f \in [L^2(\Omega)]^m$ and let $\mathcal{V} = [H^1(\Omega)]^m$ and define the subspaces

$$\mathcal{V}_g = \{v \in \mathcal{V} : \mathcal{B}v = g \text{ on } \Gamma\}, \tag{3.4}$$

and

$$\mathcal{V}_0 = \{v \in \mathcal{V} : \mathcal{B}v = 0 \text{ on } \Gamma\}. \tag{3.5}$$

Introduce the residual function $R(v)$ for problem (3.1), defined for any $v \in \mathcal{V}_g$ by

$$R(v) = \mathcal{L}v - f. \tag{3.6}$$

Note that we have $R(v) = 0$, if and only if $v = u$. Now form the functional

$$I(v) = \|R(v)\|^2 = \|\mathcal{L}v - f\|^2 \quad \text{for } v \in \mathcal{V}_g, \tag{3.7}$$

and note that

$$0 = I(u) \leq I(v) \quad \text{for all } v \in \mathcal{V}_g. \tag{3.8}$$

Thus a solution $u$ to problem (3.1) minimizes the functional $I$, and the least-squares method amounts to finding this minimizer, i.e., find $u \in \mathcal{V}_g$ such that

$$I(u) = \inf_{v \in \mathcal{V}_g} I(v). \tag{3.9}$$

A necessary condition for a function $u \in \mathcal{V}_g$ to satisfy equation (3.9), is

$$\lim_{\tau \to 0} \frac{\partial}{\partial \tau} I(u + \tau v) \equiv 2(\mathcal{L}u - f, \mathcal{L}v) = 0, \tag{3.10}$$

for all $v \in \mathcal{V}_0$.

So, the minimization of the least-squares functional $I$ leads to the variational problem: find $u \in \mathcal{V}_g$ such that

$$a(u, v) = l(v), \tag{3.11}$$

for all $v \in \mathcal{V}_0$, where

$$a(u, v) = (\mathcal{L}u, \mathcal{L}v), \tag{3.12a}$$
$$l(v) = (f, \mathcal{L}v). \tag{3.12b}$$

### 3.1.3 Weak Enforcement of Boundary Conditions

Up to now, the boundary conditions $\mathcal{B}u = g$ have been imposed strongly by restricting the space in which we seek the solution. It is also possible to impose them weakly by including equation (3.1b) in the definition of the least-squares functional. We then redefine $I(v)$ to be

$$I(v) = \alpha_1 \|\mathcal{L}v - f\|^2 + \alpha_2 \|\mathcal{B}v - g\|^2_{1/2,\Gamma} \quad \text{for } v \in \mathcal{V}, \tag{3.13}$$

Here, we need to introduce the norm $\|\cdot\|_{1/2,\Gamma}$ in order to get a consistent functional. Also note that we have introduced the parameters $\alpha_1, \alpha_2 > 0$ to indicate that we have a choice in how the different contributions are weighted in the functional.

Seeking a minimizer to $I$ in $\mathcal{V}$ leads to the following variational problem: find $u \in \mathcal{V}$ such that

$$a(u, v) = l(v), \tag{3.14}$$

for all $v \in \mathcal{V}$, where

$$a(u, v) = (\mathcal{L}u, \mathcal{L}v) + (\mathcal{B}u, \mathcal{B}v)_{1/2,\Gamma}, \tag{3.15a}$$
$$l(v) = (f, \mathcal{L}v) + (g, \mathcal{B}v)_{1/2,\Gamma}. \tag{3.15b}$$

### 3.1.4 The Least-Squares Finite Element Method

Let $\mathcal{T}_h$ be a decomposition of the domain $\Omega$ into, e.g., tetrahedral, finite elements $K$. The index $h$ denotes the mesh function and is a measure of the local size of the elements in the mesh, $h|_K = \operatorname{diam}(K)$, and we also assume a minimal angle condition on the triangulation, see Brenner and Scott [10]. We introduce a global mesh parameter $\hat{h} = \max_{K \in \mathcal{T}_h} h(K)$. Define

$$\mathcal{V}_h = \{u_h \in [C^0(\overline{\Omega})]^m : u_h|_K \in \mathcal{P}_r(K), \text{for all } K \in \mathcal{T}_h\} \quad \text{with } r \geq 1,$$

associated with this triangulation, where $\mathcal{P}_r$ is the set of all vector polynomials of degree less than or equal to $r$. Thus $\mathcal{V}_h$ is the set of all continuous piecewise vector polynomial functions $u_h$ such that, in each element, $u_h \in \mathcal{P}_r$.

For the error analysis following below, we need the following approximation property of $\mathcal{V}_h$, see, e.g., [10] for a proof. Given a function $u \in [H^{r+1}(\Omega)]^m$ with $r \geq 1$, there exists a function $v_h \in \mathcal{V}_h$ such that

$$\|u - v_h\|_s \leq C\hat{h}^{r+1-s}\|u\|_{r+1}, \quad s = 0, 1, \tag{3.16}$$

where the constant C is independent of the global mesh size $\hat{h}$.

Assuming that $g$ can be exactly represented by continuous piecewise polynomials, and if not, replacing it by its $L^2$ projection $Pg$, we define the finite element subspace $\mathcal{V}_{h,g}$ of $\mathcal{V}_g$ by $\mathcal{V}_{h,g} = \mathcal{V}_h \cap \mathcal{V}_g$, and similarly we define $\mathcal{V}_{h,0} = \mathcal{V}_h \cap \mathcal{V}_0$.

The least-squares finite element method (LSFEM) corresponding to (3.9) can now be formulated by restricting the minimization problem: find $u \in \mathcal{V}_{h,g}$ such that

$$I(u) = \inf_{v \in \mathcal{V}_{h,g}} I(v). \tag{3.17}$$

Necessary conditions for a minimum in $\mathcal{V}_{h,g}$ lead to the variational problem: find $u_h \in \mathcal{V}_{h,g}$ such that

$$a(u_h, v) = l(v), \tag{3.18}$$

for all $v \in \mathcal{V}_{h,0}$, where $a(\cdot,\cdot)$ and $l(\cdot)$ are defined as in equation (3.12).

For the solution $u$ to (3.11), we also have

$$a(u, v) = l(v) \quad \text{for all } v \in \mathcal{V}_{h,0}, \tag{3.19}$$

since $\mathcal{V}_{h,0} \subset \mathcal{V}_0$. Subtracting equation (3.18) from equation (3.19), we obtain the Galerkin orthogonality

$$a(u - u_h, v) = 0 \quad \text{for all } v \in \mathcal{V}_{h,0}. \tag{3.20}$$

When LSFEM is formulated with weak enforcement of boundary conditions, it takes the form: find $u_h \in \mathcal{V}_h$ such that

$$a(u_h, v) = l(v), \tag{3.21}$$

for all $v \in \mathcal{V}_h$,where now $a(\cdot,\cdot)$ and $l(\cdot)$ are defined as in equation (3.15), and we have the corresponding Galerkin orthogonality

$$a(u - u_h, v) = 0 \quad \text{for all } v \in \mathcal{V}_h. \tag{3.22}$$

Furthermore, the inner product $(\cdot,\cdot)_{1/2,\Gamma}$ and corresponding norm $\|\cdot\|_{1/2,\Gamma}$, and can preferably be replaced by the more easily computed weighted mesh dependent $L^2$ inner product $(\cdot,\cdot)_{\Gamma,h^{-1}}$ and norm $\|\cdot\|_{\Gamma,h^{-1}}$, where $h$ denotes the local mesh function, see [17], [30].

### 3.1.5 A Priori Error Estimates

Before we state the error estimate, we introduce the energy norm,

$$|||v|||^2 = a(v, v) \quad \text{for } v \in \mathcal{V}, \tag{3.23}$$

Under our assumptions, this is a norm in $\mathcal{V}_0$, which we now show.

**Lemma 3.1.1** *If there exists a unique solution to problem (3.1), then the energy norm, as defined by (3.23), is a norm in* $\mathcal{V}_0$.

**Proof.** What needs to be proved is that

$$|||v||| = 0 \quad \Rightarrow \quad v = 0 \quad \text{for } v \in \mathcal{V}_0. \tag{3.24}$$

But from the assumptions we know that the homogeneous problem

$$\mathcal{L}v = 0 \quad \text{in } \Omega, \tag{3.25a}$$
$$\mathcal{B}v = 0 \quad \text{on } \Gamma, \tag{3.25b}$$

has a unique solution $v \equiv 0$. □

**Remark 3.1.1.** In the case of weak enforcement of boundary conditions, i.e., $a(\cdot, \cdot)$ is defined by (3.15), the energy norm is indeed a norm on the whole space $\mathcal{V}$. □

Now we are ready to state the following result:

**Theorem 3.1.2 (A Priori Error Estimate for LSFEM)** *Let* $u \in \mathcal{V} = [H^1(\Omega)]^m$ *be a solution to problem 3.1, where* $\mathcal{L}$ *is a linear first order differential operator. For an approximate solution* $u_h \in \mathcal{V}_h$ *obtained by LSFEM, as defined by equation (3.18) or (3.21), there is a constant* $C$*, independent of* $u$ *and* $h$*, such that*

$$|||u - u_h||| \le C\hat{h}^r |u|_{r+1}. \tag{3.26}$$

**Proof.** Let $v_h$ be an arbitrary function in $\mathcal{V}_{h,g}$ and let $e = u - u_h$ denote the error. Then

$$\begin{aligned} |||e|||^2 &= a(e, u - u_h) \\ &= a(e, u - v_h + v_h - u_h) \\ &= a(e, u - v_h), \end{aligned} \tag{3.27}$$

where (3.20) (or (3.22)) was used in the last equality. Using the Cauchy-Schwartz inequality and dividing by $|||e|||$ we arrive at

$$|||e||| \leq |||u - v_h|||. \tag{3.28}$$

Further,

$$|||u - v_h||| \leq C\|u - v_h\|_1, \tag{3.29}$$

which follows from the form of $\mathcal{L}$, as defined by equation (3.2), using the assumptions on the coefficients. The interpolation error estimate (3.16) gives the result. □

**Remark 3.1.2.** Note that, considering the case of strong enforcement of the boundary conditions,

$$|||u - u_h||| = \|\mathcal{L}(u - u_h)\| = \|f - \mathcal{L}u_h\| = \| - R(u_h)\|. \tag{3.30}$$

Thus we also have

$$\|R(u_h)\| \leq C\hat{h}^r |u|_{r+1}. \tag{3.31}$$

A corresponding estimate in the case of weakly imposed boundary conditions also holds. □

### 3.1.6 A Priori Error Estimates for Elliptic Problems

Moreover, for elliptic problems, it is possible to derive an improved result. We say that the problem is elliptic if the bilinear form $a(\cdot, \cdot)$ is coercive with respect to the $H^1$ norm, which coincides with the definition used in section 2.4.2. In other words,

$$\alpha\|v\|_1^2 \leq a(v, v) \tag{3.32}$$

for $v \in \mathcal{V}_0$ when boundary conditions are imposed strongly, and for $v \in \mathcal{V}$ when they are imposed weakly.

**Theorem 3.1.3** *Let $u \in \mathcal{V} = [H^1(\Omega)]^m$ be a solution to problem (3.1), where $\mathcal{L}$ is a continuous linear first order elliptic differential operator. For an approximate solution $u_h \in \mathcal{V}_h$ obtained by LSFEM, as defined by equation (3.18) or (3.21), there are constants $C_1$ and $C_2$ independent of $u$ and $h$ such that*

$$\|u - u_h\|_1 \leq C_1\hat{h}^r |u|_{r+1}, \tag{3.33}$$

*and*

$$\|u - u_h\| \leq C_2\hat{h}^{r+1} |u|_{r+1}, \tag{3.34}$$

*where for (3.34) we also assume that the regularity estimate (3.39) below holds.*

**Proof.** The estimate (3.33) follows directly from (3.32) and Theorem 3.1.2.

To prove (3.34) we adopt the Aubin-Nitsche trick, as in [23], and introduce the dual problem: find $\phi \in \mathcal{V}_0$, such that

$$a(\phi, v) = (e, v), \tag{3.35}$$

for all $v \in \mathcal{V}_0$. Chosing $v = e$, we get

$$\begin{aligned} \|e\|^2 &= (e, e, ) \\ &= a(e, \phi) \\ &= a(e, \phi - \phi_h) \\ &\leq |||e|||\ |||\phi - \phi_h|||, \end{aligned} \tag{3.36}$$

where we have introduced $\phi_h \in \mathcal{V}_{h,0}$, and made use of equations (3.35), (3.20) (or (3.22)) and finally the Cauchy-Schwartz inequality.

From the energy norm estimate (3.26), we have

$$\|e\|^2 \leq C\hat{h}^r |u|_{r+1}\, |||\phi - \phi_h|||. \tag{3.37}$$

Furthermore,

$$|||\phi - \phi_h||| \leq C\|\phi - \phi_h\|_1 \leq C\hat{h}|\phi|_2, \tag{3.38}$$

where the last step follows from the interpolation error estimate (3.16). Using elliptic regularity for $\phi$,

$$|\phi|_2 \leq C\|e\|, \tag{3.39}$$

we thus arrive at

$$\begin{aligned} \|e\|^2 &\leq C\hat{h}^{r+1}|u|_{r+1}|\phi|_2 \\ &= C\hat{h}^{r+1}|u|_{r+1}\|e\|, \end{aligned} \tag{3.40}$$

which, after division with $\|e\|$, gives the desired result. □

### 3.1.7 Residual Based A Posteriori Estimates

In Remark 3.1.2, we observed that

$$|||u - u_h||| = \|R(u_h)\|. \tag{3.41}$$

Here expressed for strongly imposed boundary conditions; in the case of weak enforcement of boundary conditions, a corresponding boundary residual term would appear on the right hand side.

Hence, the energy norm of the error is a computable quantity. Furthermore, in the following sections we will state the coercivity for $a(\cdot, \cdot)$ for some examples, i.e.,

$$C\|v\|_s^2 \leq a(v, v), \tag{3.42}$$

where $s$ depends on the problem and the least-squares formulation. It is then possible to give an a posteriori error estimate in the norm in which we can show the coercivity, since

$$\|u - u_h\|_s^2 \leq Ca(u - u_h, u - u_h) = |||u - u_h|||^2 = \|R(u_h)\|^2. \tag{3.43}$$

## 3.2 A First Example: Pure Scalar Convection

As a simple example, we start by studying the following boundary value problem:

$$\beta \cdot \nabla u = f \quad \text{in } \Omega, \tag{3.44a}$$

$$u = 0 \quad \text{on } \Gamma_{inflow}, \tag{3.44b}$$

where $\beta \in \mathbf{R}^3$ is a flow vector, and $\Gamma_{inflow}$ is the part of the boundary where $\beta \cdot n < 0$ for the exterior unit normal $n$ to the boundary $\Gamma$. Here, typically, $u$ models the concentration of a substance in a fluid with the flow given by $\beta$. An attempt to solve this problem directly by the standard Galerkin finite element method, will lead to the well known problem of oscillatory solutions due to the odd-even coupling of the unknown nodal values, see, e.g., [13].

Formulating LSFEM for (3.44) gives: find $u_h \in \mathcal{V}_{h,0}$, such that

$$(\beta \cdot \nabla u_h, \beta \cdot \nabla v) = (f, \beta \cdot \nabla v), \tag{3.45}$$

for all $v \in \mathcal{V}_{h,0}$, where $\mathcal{V}_{h,0}$ is defined as in section 3.1.4.

Applying Theorem 3.1.2 for the presented formulation, gives the error estimate

$$|||u - u_h||| \leq C\hat{h}^r |u|_{r+1}. \tag{3.46}$$

By the Poincaré-Friedrichs inequality, see, e.g., [13] or [18] we can get the following lower bounded for the energy norm,

$$\|u - u_h\|^2 + \|\beta \cdot \nabla(u - u_h)\|^2 \leq C|||u - u_h|||^2. \tag{3.47}$$

We thus get the error estimate

$$\|u - u_h\| + \|\beta \cdot \nabla(u - u_h)\|^2 \leq C\hat{h}^r |u|_{r+1}. \tag{3.48}$$

Thus, the least-squares finite element method applied to this first order problem leads to a stable symmetric positive definite discrete system and no need for stabilizing or upwinding terms are necessary. Note however, that the error estimate (3.48) is suboptimal.

## 3.3 Application to a Second Order Problem: Poisson's Equation

One of the most common equations used in mathematical modelling is the Poisson equation,

$$-\Delta u = f \quad \text{in } \Omega, \tag{3.49a}$$
$$u = 0 \quad \text{on } \Gamma. \tag{3.49b}$$

Here, $u$ may model, e.g., heat conduction, diffusion of a chemical substance or displacement in an elastic material.

Following the previous sections, we formulate this as a first order system. This is also motivated, since one is often not primarily interested in the solution by itself, but rather the gradient of it. In the examples mentioned above it would be the fluxes or the strain.

Introducing $\sigma = -\nabla u$, we rewrite (3.49) and get

$$\nabla \cdot \sigma = f \quad \text{in } \Omega, \tag{3.50a}$$
$$\sigma + \nabla u = 0 \quad \text{in } \Omega, \tag{3.50b}$$
$$u = 0 \quad \text{on } \Gamma. \tag{3.50c}$$

This first order system is not straight-forward to solve by the Galerkin approach, but it is now in a form suitable for LSFEM.

We form the least-squares functional as

$$I(\sigma, u) = \|\nabla \cdot \sigma - f\|^2 + \|\sigma + \nabla u\|^2. \tag{3.51}$$

Seeking a minimizer to equation (3.51) leads to the variational problem: find $(\sigma, u) \in \mathcal{V}_0 = \{(\delta, v) \in H_{div} \times H^1 : v = 0 \text{ on } \Gamma\}$ such that

$$(\nabla \cdot \sigma, \nabla \cdot \tilde{\sigma}) + (\sigma + \nabla u, \tilde{\sigma} + \nabla \tilde{u}) = (f, \nabla \cdot \tilde{\sigma}), \tag{3.52}$$

for all $(\tilde{\sigma}, \tilde{u}) \in \mathcal{V}_0$. LSFEM amounts to seeking a solution $(\sigma_h, u_h) \in \mathcal{V}_{h,0}$, satisfying equation (3.52) for all $(\tilde{\sigma}, \tilde{u}) \in \mathcal{V}_{h,0}$.

Theorem 3.1.2 yields the following estimate for this formulation,

$$|||(\sigma - \sigma_h, u - u_h)||| \leq C\hat{h}^r(\|\sigma\|_{r+1} + \|u\|_{r+1}). \tag{3.53}$$

Furthermore, we can obtain, see [18], [25], the bound

$$\|\sigma - \sigma_h\|_{H_{div}} + \|u - u_h\|_1 \leq C|||(\sigma - \sigma_h, u - u_h)|||. \tag{3.54}$$

Combining (3.53) and (3.54) yields the estimate

$$\|\sigma - \sigma_h\|_{H_{div}} + \|u - u_h\|_1 \leq C\hat{h}^r(\|\sigma\|_{r+1} + \|u\|_{r+1}), \tag{3.55}$$

which is suboptimal since we only get a bound on the divergence of $\sigma$, and not the full $H^1$ bound.

It is however possible to achieve this $H^1$ boundedness by adding a consistent constraint, or penalty term, on the curl of $\sigma$. Since $\nabla \times \nabla v = 0$ for any sufficiently smooth function $v$, we know that

$$\nabla \times \sigma = 0.$$

These equations are easily added to our system, leading to the functional

$$I(\sigma, u) = \|\nabla \cdot \sigma - f\|^2 + \|\sigma + \nabla u\|^2 + \|\nabla \times \sigma\|^2, \tag{3.56}$$

and the variational problem becomes: find $(\sigma, u) \in \mathcal{V}_0 = \{(\delta, v) \in [H^1]^3 \times H^1 : v = 0 \text{ on } \Gamma\}$ such that

$$(\nabla \cdot \sigma, \nabla \cdot \tilde{\sigma}) + (\sigma + \nabla u, \tilde{\sigma} + \nabla \tilde{u}) + (\nabla \times \sigma, \nabla \times \tilde{\sigma}) = (f, \nabla \cdot \tilde{\sigma}), \tag{3.57}$$

for all $(\tilde{\sigma}, \tilde{u}) \in \mathcal{V}_0$. Then $H^1$ coercivity can be established, see [23], [25], resulting in the error estimate,

$$\|\sigma - \sigma_h\|_1 + \|u - u_h\|_1 \leq C\hat{h}^r(\|\sigma\|_{r+1} + \|u\|_{r+1}). \tag{3.58}$$

This example shows that, even if the least-squares method is straightforward, the most obvius approach may not lead to the best formulation. Instead one may have to play a little with the set-up of the problem. However, it also shows that these manipulations are easy to do; adding three equations did not complicate matters.

**Remark 3.3.1.** In the analysis in section 3.1, we assumed that the differential operator $\mathcal{L}$ was first order. This is not necessary for LSFEM, but the methodology is not practicle for higher order problems.

Applying LSFEM directly to problem (3.49) yields: find $u \in \mathcal{V}_0 = \{v \in H^1 : v = 0 \text{ on } \Gamma\}$, such that

$$(\Delta u, \Delta v) = (f, \Delta v), \tag{3.59}$$

for all $v \in \mathcal{V}_0$. We would in this case have to use finite element functions $v \in C^1(\overline{\Omega})$, which for triangulations in two dimensions require polynomials of degree five or higher, see, e.g., [10]. □

## 3.4 Application to a First Order System: Magnetostatics

The magnetostatic equations (2.11) can be written

$$\nabla \times \frac{B}{\mu} = J \quad \text{in } \Omega, \tag{3.60a}$$

$$\nabla \cdot B = 0 \quad \text{in } \Omega, \tag{3.60b}$$

$$n \cdot B = 0 \quad \text{on } \Gamma, \tag{3.60c}$$

where we used the constitutive relation (2.2) to eliminate $H$.

This system is first-order, with four equations and three unknowns. The complication of having one more equation than unknowns has lead to several attempts of reformulating this system. The occurrence of spurious, non-physical solutions in many of these attempts is probably due to disregarding the importance of the divergence equation, see [18], [3].

In LSFEM, however, there is no problem in having more equations than unknowns. So, to first put this in the div-curl framework, we assume constant material parameters and form the following functional

$$I(B) = \|\nabla \times B - \mu J\|^2 + \|\nabla \cdot B\|^2, \tag{3.61}$$

where we multiplied the first equation with $\mu$. The corresponding weak form is

$$(\nabla \times B, \nabla \times \tilde{B}) + (\nabla \cdot B, \nabla \cdot \tilde{B}) = (\mu J, \nabla \times \tilde{B}), \tag{3.62}$$

and the least-squares finite element method is: find $B_h \in \mathcal{V}_{h,0} \subset \mathcal{V}_0 = \{v \in [H^1(\Omega)]^3 : n \cdot v = 0 \text{ on } \Gamma\}$, such that equation (3.62) is satisfied for all $\tilde{B} \in \mathcal{V}_{h,0}$.

From Lemma 2.4.2, we know that this bilinear form is $H^1$ coercive. This, combined with Theorem 3.1.3, gives the a priori error bound

$$\|B - B_h\|_1 \leq C\hat{h}^r |B|_{r+1}. \tag{3.63}$$

If we consider instead the more interesting case of piecewise constant constitutive parameters, thus introducing magnetic materials in the problem, the situation is slightly different. The interface conditions (2.3) is a complication that is quite specific to Maxwell's equations formulated in the primary field variables. It is handled by introducing discontinuous elements on the interface surfaces and applying the algebraic conditions in either a weak or a strong form.

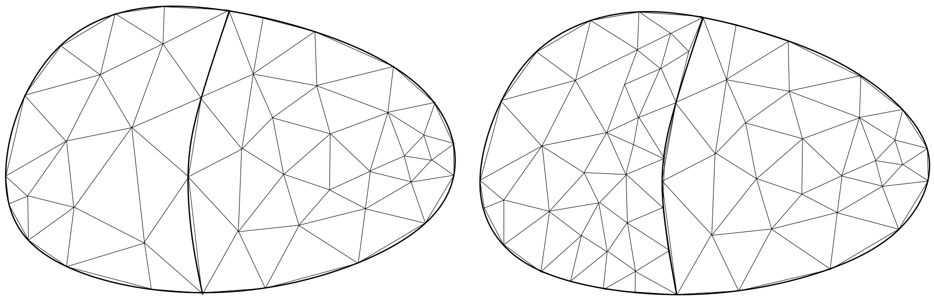

(a) *Conforming triangulation* (b) *Non-conforming triangulation*

Figure 3.1: Examples of conforming and non-conforming triangulations of two subdomains. In the first case, we have the choice of both strong and weak enforcement of interface conditions. For the non-conforming grid, however, we must use weak enforcement.

In the case of strong enforcement of the interface conditions, we make a coordinate transformation of the problem at the nodes lying on a surface; instead of expressing the unknowns in cartesian coordinates, we calculate an orthogonal coordinate system using the normal and tangent vectors for the surface. For each node, we then explicitly eliminate the degrees of freedoms on one side of the surface using the algebraic equations (2.3).

The weak implementation is less complex, and simply consists of computing the surface integrals introduced in the variational formulation. Note that in the case of strong enforcement, the meshes used must be conforming on the interface, i.e., the surface nodes for the meshes must coincide and the same interpolating functions must be used. This is not necessary when imposing the conditions weakly. We may then use both non-conforming grids and different finite element functions, see Figure 3.1.

So, assume that $\Omega = \bigcup_{i=1}^{n} \Omega^i$, where each subdomain have the magnetic permeability $\mu|_{\Omega^i} = \mu_r^i\,\mu_0$, let $\mathcal{V}^i = [H^1(\Omega^i)]^3$ and denote the interface between regions $\Omega^i$ and $\Omega^j$ by $\Gamma^{ij}$, see Figure 3.2.

We now write the system as

$$\nabla \times \frac{B}{\mu} = J \quad \text{in } \Omega^i, \tag{3.64a}$$

$$\nabla \cdot B = 0 \quad \text{in } \Omega^i, \tag{3.64b}$$

$$n \cdot B = 0 \quad \text{on } \Gamma, \tag{3.64c}$$

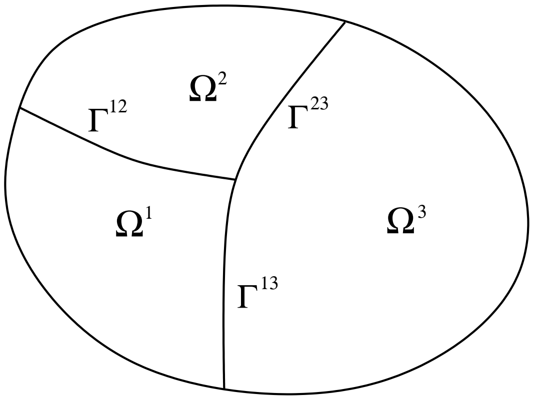


Figure 3.2: The notation used when a region is split into subregions.

together with the interface conditions

$$[\frac{B}{\mu}] \times n = 0 \quad \text{on } \Gamma^{ij}, \tag{3.65a}$$

$$[B] \cdot n = 0 \quad \text{on } \Gamma^{ij}, \tag{3.65b}$$

where $[\cdot]$ denotes the jump, and $n$ is a unit normal to the surface.

Choosing to impose conditions (3.65) and the boundary condition (3.64c) weakly, we form the least-squares functional

$$\begin{aligned} I(B) = \alpha_1 \Big( \sum_{i=1}^{n} \|\mu(\nabla \times \frac{B}{\mu} - J)\|^2_{\Omega^i} + \|\nabla \cdot B\|^2_{\Omega^i} \Big) \\ + \alpha_2 \Big( \sum_{1 \le i < j \le n} \big( \|\tilde{\mu}[n \times \frac{B}{\mu}]\|^2_{1/2,\Gamma^{ij}} + \|[n \cdot B]\|^2_{1/2,\Gamma^{ij}} \big) \\ + \|[n \cdot B]\|^2_{1/2,\Gamma} \Big). \end{aligned} \tag{3.66}$$

The parameter $\tilde{\mu}$ corresponds to the multiplication with $\mu$ in the volume integrals, but is an average value since $\mu$ is not defined on the interface.

We introduce the finite element subspaces $\mathcal{V}_h^i \subset \mathcal{V}^i$ where the degree of the polynomial basis functions thus may be different in different subregions, and define $\mathcal{V}_h = \bigcup_{i=1}^n \mathcal{V}_h^i$.

Based on the functional (3.66), we can now formulate LSFEM for the magnetostatic problem (3.60): find $B_h \in \mathcal{V}_h$ such that

$$\alpha_1 \, a_\Omega(B_h, \tilde{B}) + \alpha_2 \, a_\Gamma(B_h, \tilde{B}) = \alpha_1 \, l(\tilde{B}), \tag{3.67}$$

for all $\tilde{B} \in \mathcal{V}_h$, where

$$a_\Omega(B_h, \tilde{B}) = \sum_{i=1}^{n}(\mu\nabla \times \frac{B_h}{\mu}, \mu\nabla \times \frac{\tilde{B}}{\mu})_{\Omega^i} + (\nabla \cdot B_h, \nabla \cdot \tilde{B})_{\Omega^i}, \tag{3.68a}$$

$$\begin{aligned} a_\Gamma(B_h, \tilde{B}) = & \sum_{1 \le i < j \le n} \Big( (\tilde{\mu}[n \times \frac{B_h}{\mu}], \tilde{\mu}[n \times \frac{\tilde{B}}{\mu}])_{\Gamma^{ij}, h^{-1}} \\ & + ([n \cdot B_h], [n \cdot \tilde{B}])_{\Gamma^{ij}, h^{-1}} \Big) + ([n \cdot B_h], [n \cdot \tilde{B}])_{\Gamma, h^{-1}}, \end{aligned} \tag{3.68b}$$

$$l(\tilde{B}) = \sum_{i=1}^{n}(J, \mu\nabla \times \frac{\tilde{B}}{\mu})_{\Omega^i}. \tag{3.68c}$$

Here we have used the weighted boundary inner products introduced in section 3.1.4.

In each subdomain, Lemma 2.4.2 is valid, leading to the inequality

$$\sum_{i=1}^{n} \|B - B_h\|^2_{1,\Omega^i} \le |||B - B_h|||^2. \tag{3.69}$$

Furthermore, in [16], Ivarsson constructs, as in [27], an interpolation operator that preserves the interface conditions, thus, using the same technique as in the proof of Theorem 3.1.3, we can show

$$\Big( \sum_{i=1}^{n} \|B - B_h\|^2_{1,\Omega^i} \Big)^{1/2} \le C\hat{h}^r |B|_{r+1}. \tag{3.70}$$

# Chapter 4

# Software

The software used in this work consists of three parts: a preprocessor to define the geometry and generate an initial computational grid, a FEM solver, and a postprocessor to visualize the results and to compute derived quantities. The FEM solver that has been developed builds on the platform of Chalmers Finite Element Center, while commercial software has been used for pre- and postprocessing.

The solver by itself consists of several components. The first is the discretization of the continuous equations into a system of algebraic equations. The second is a solver for this discrete problem. A third component, vital when adaptively refining the computational mesh, is a set of routines to handle the hierarchy of meshes and the coupling to the geometry.

In the following sections, these components will be presented in some detail.

## 4.1 Discretization of the Variational Formulation

As one aim of this work was to numerically study several different formulations, it has been important to develop a tool where the problem formulation was easily accessible. The resulting discretizer consists of a set of C++ routines that assemble a matrix based on a given variational formulation.

The functionality and level of abstraction in C++ have made it possible to make this process very similar to the analytical mathematical formulation. As an example, take the Poisson equation,

$$-\Delta u = f,$$

with some boundary conditions, which we for simplicity ignore in this discussion. The variational formulation for this problem is: find $u$ such that

$$(\nabla u, \nabla v) = (f, v),$$

for all $v$. The left hand side, expanded in cartesian coordinates, takes the form

$$(\nabla u, \nabla v) = \int_\Omega (u_x v_x + u_y v_y + u_z v_z)\ d\Omega.$$

In C++, the corresponding expression is coded

```
u.x()*v.x() + u.y()*v.y() + u.z()*v.z().
```

The computer code is thus very close to the mathematical formulation, making it easy to read and set up new problems.

It has also been easy to add new elements, e.g. higher order polynomials and edge elements, or quadrature rules. The code is also independent of space dimensionality and the routines have been parallelized. The drawback of this very general approach is the difficulties with efficiency; it is possible to do more optimization for a specific application than in the general case. The choice of C++ is based on the combination of a high level of abstraction and reasonable numerical efficiency.

Similar general approaches with finite element codes in C++ have been reported by, e.g., Jiao [20] and Langtangen [21].

## 4.2 Solving the Discrete Problem

For this task, we utilize a free software package called PETSc, see [4], [5], and [6]. This package provides a large range of iterative solvers and preconditioners together with a storage format for sparse matrices. These tools are designed for use on both single processor computers, as well as on parallel ones. Altough some suboptimal implementations have been discovered, we find that PETSc has been a powerful tool, well suited for our needs.

## 4.3 CAD, Geometry, and Meshes

Even if the geometry and initial mesh is constructed in the preprocessor stage as mentioned above, it is for several reasons important to establish a relation between the geometry and the mesh, and transfer this relation into the equation solving step. Unfortunately, the mesh generator does often not supply this relation and once the surface mesh is generated it disregards the geometry description. Therefore, one has to make a new identification between the mesh and the geometry.

The way this is done, is to import not only the computational grid, but also the geometry description used to generate it. Nodes on and elements adjacent to surfaces are identified by the following algorithm:

*Compute, in an efficient manner, the distances between each triangulation and each geometry. The pair with smallest distance is identified and thereby the geometry connection is decided.*

The most important use of this relation is for adaptive mesh refinement. As the discrete problem tend to get very large in three space dimensions, adaptive refinement of the computational grid is vital in order to get reasonable accuracy. One starts with a coarse mesh generated from a description of the geometry. Based on the computed solution, one splits elements only where it has most effect.

In order to achieve improved accuracy when refining, it is important that the nodes in the new elements are fitted to the original geometry. In general, when an element is splitted in the refinement process, a new node is placed on the midpoint of the edge in the old element. If this edge is part of a curved surface, the new node has to be moved in order to lie on the surface. This idea is illustrated in two dimensions in Figure 4.1. How this has worked in practice is shown in Figure 4.2, where part of the mesh for the iron core in Problem 1 is shown before and after adaptive refinement.

Another important usage in these electromagnetic applications is to compute normal and tangent vectors, used in the boundary and interface conditions. Nodal values for these vectors can now be computed using the geometry description instead of taking some average of the values for the faces surrounding the node.

The geometry routines described above have been developed by Klas Samuelsson at Chalmers Finite Element center within an ITM project. For more details on their construction and usage, see the ITM Technical Report [7].

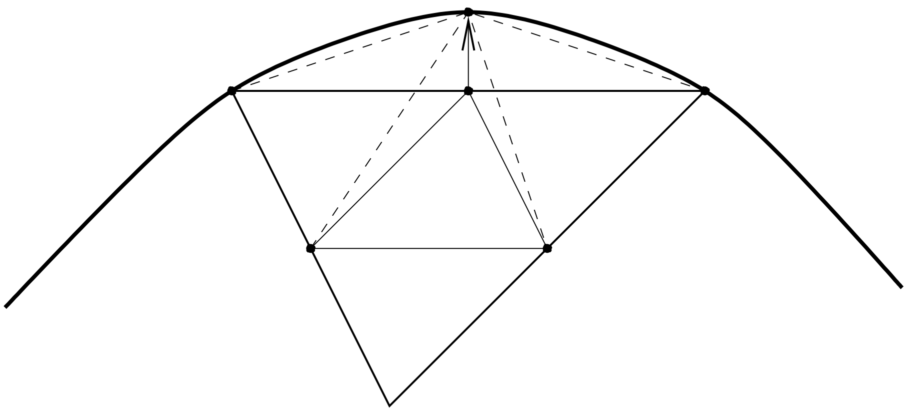

Figure 4.1: A schematic picture showing the projection of a new node on to a curved boundary.

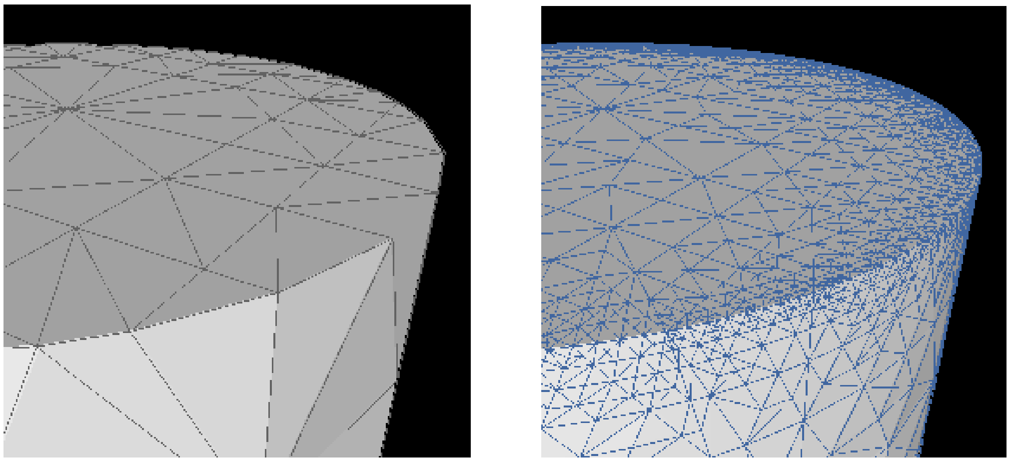

Figure 4.2: Example of an adaptive mesh refinement, using the geometry description from the CAD model to project the new nodes on to the curved surface.

# Chapter 5

# Numerical Examples

## 5.1 General Considerations

### 5.1.1 Implementation of Boundary and Interface Conditions

The discontinuity of the field variables have numerically been handled by introducing discontinuous finite elements on the surfaces. The algebraic conditions in equation (2.3) are enforced either strongly, by eliminating the extra degrees of freedom, or weakly, by adding terms to the least-squares functional as described in section 3.4.

The strong implementation consists of first identifying elements with an element face lying in a surface, and for each node on this face, making the coordinate transformation for the element stiffness matrix before adding it to the global matrix. The degrees of freedom on one side of the surface are then eliminated from the discrete linear system of equations. When the solution has been computed, it needs to be transformed back into cartesian coordinates and expanded to include the eliminated degrees of freedom.

The weak implementation is less complex, and simply consists of computing the surface integrals introduced in the least-squares residual. The identification of element faces lying in the surface is done also in this case, but no change of coordinate system is needed. Instead, a face stiffness matrix is computed and added to the global matrix.

Since we introduce extra degrees of freedoms in the weak implementation, it leads to slightly larger matrix problems. However, the strong implementation is more costly to compute. In both case we make use of the normal vectors computed from the CAD model as described in section 4.3.

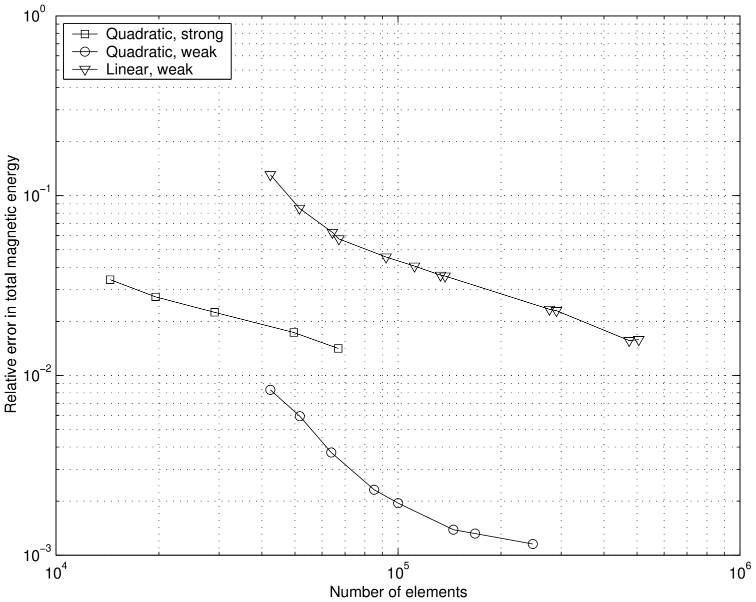


Figure 5.1: Comparison of convergence between strong and weak implementation of boundary conditions in Problem 1.

### 5.1.2 Strong or Weak Enforcement of Boundary and Interface Conditions

For all the numerical results presented in the following sections, we have used weak enforcement of boundary and interface conditions with the extra residual terms weighted by the parameter $\alpha_i = 10$. Strong implementation of the boundary/interface conditions have been tested, but seems to be more sensitive to singularities, with considerably slower convergence compared with weak implementation, see Figure 5.1. From the figure we can see that the convergence order seem to be approximately the same for strong implementation with quadratic polynomials as in the case of weak enforcement of interface conditions with linear polynomials, though the error is smaller in the first case.

The explanation to this is probably that the conflict in the interface conditions at a corner or edge, which is the cause of the singularities, is transferred to the discrete problem when using strong enforcement of the algebraic conditions. It should be mentioned though, that in the implementation, the elementwise transformation leads to an averaging of the normal in the corner and thus "softening" the conflicting conditions.

The values of $\alpha_i$ have been chosen as large as possible without affecting the condition number of the matrix seriously. As $\alpha$ tends to infinity we would, in theory, get the conditions strongly imposed.

### 5.1.3 Adaptive Mesh Refinement Criteria

The natural indicator to base the adaptivity on is the least-square residual. But in the presence of corner singularities, the discrete residual actually increases when refining the mesh, making it inapropriate as an indicator.

Instead we have for the static problems used the elementwise indicator

$$I_K = \|h\nabla \cdot B\|_K^2, \tag{5.1}$$

where $h$ indicates the local mesh function, as an indicator of where to refine.

In the time harmonic example, no magnetic materials where present and no problem with increasing least-squares residual occurred. Consequently, the element residual

$$\begin{aligned} I_K = &\|h(\nabla \times E + j\omega\mu H)\|_K^2 \\ &+ \|h(\nabla \times H - \sigma E - J_{sc})\|_K^2 \\ &+ \|h\nabla \cdot (\mu H)\|_K^2, \end{aligned} \tag{5.2}$$

where $h$ indicates the local mesh function, could be used successfully.

From section 3.1.7, we know that the residual is equal to the energy norm of the problem, making it an appropriate indicator by itself. However, the weighting with $h$ in these indicators was done to soften the criteria somewhat.

## 5.2 Problem 1: A Magnetostatic Problem

### 5.2.1 Description of the Problem

The geometry of this problem is described in Figure 5.2. The problem is axisymmetric in order to make two dimensional computations possible for reference solutions. A three dimensional view can be seen in Figure 5.3. The model consists of an iron cylinder core inserted in a copper winding. The configuration is enclosed in air and surrounded by a box with perfectly conducting surfaces. The winding is modeled as a homogeneous copper coil.

Data for this problem are that the relative magnetic permeabilities are $\mu_{r,Fe} = 10^4$ and $\mu_{r,Cu} = \mu_{r,air} = 1$ and $\mu_0 = 4\pi \times 10^{-7}$ H/m and the current density $J$ is constant over the cross section of the coil and the total current is 1 A.

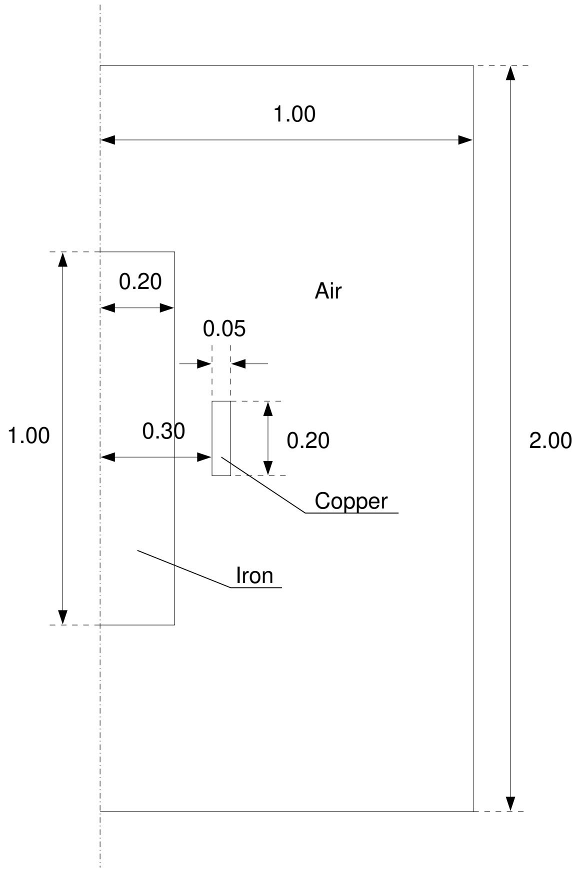


Figure 5.2: The geometry of the axisymmetric Problem 1. The dimensions are given in meters.

Reference computations in two dimensions done by ABB and reported in [7], gave the values of the magnetic energies in the different materials as listed in Table 5.1, where the magnetic energy is defined by

$$W_\Omega = \frac{1}{2}\int_\Omega B \cdot H \, d\Omega. \tag{5.3}$$

### 5.2.2 The Equations

The equations solved are the magnetostatic equations:

$$\nabla \times H = J, \tag{5.4a}$$
$$\nabla \cdot B = 0, \tag{5.4b}$$

in each subdomain, where

$$B = \mu_r \mu_0 H, \tag{5.5}$$

subject to the interface conditions

$$[B] \cdot n = 0, \tag{5.6a}$$
$$[H] \times n = 0, \tag{5.6b}$$

on all internal boundaries, where $[\cdot]$ denotes the jump across the surface and $n$ is a unit normal to the surface. The boundary condition

$$B \cdot n = 0, \tag{5.7}$$

has been used on the outer boundary.

### 5.2.3 The Least-Squares Formulation

Using equation (5.5) to eliminate $H$, the least squares functional takes the form

$$\begin{aligned} I(B) = \sum_{i=1}^{3} \left( \|\nabla \times \frac{B}{\mu_i} - J\|^2_{\Omega^i,\mu_i^2} + \|\nabla \cdot B\|^2_{\Omega^i} \right) \\ + \alpha_1 \sum_{1 \le i < j \le 3} \left( \|[n \times \frac{B}{\mu}]\|^2_{\Gamma^{ij},\tilde{\mu}^2 h^{-1}} + \|[n \cdot B]\|^2_{\Gamma^{ij},h^{-1}} \right) \\ + \alpha_2 \|[n \cdot B]\|^2_{\Gamma,h^{-1}}, \end{aligned} \tag{5.8}$$

where the weighted norm is defined by

$$\|v\|^2_{\Omega,\omega} = \int_\Omega v^2 \omega \, d\Omega.$$

The resulting variational formulation then becomes: find $B$, such that

$$a_\Omega(B,\tilde{B}) + \alpha_1 \, a_1(B,\tilde{B}) + \alpha_2 \, a_2(B,\tilde{B}) = l(\tilde{B}), \tag{5.9}$$

for all $\tilde{B}$, where

$$a_\Omega(B,\tilde{B}) = \sum_{i=1}^{3} (\mu\nabla \times \frac{B}{\mu}, \mu\nabla \times \frac{\tilde{B}}{\mu})_{\Omega^i} + (\nabla \cdot B, \nabla \cdot \tilde{B})_{\Omega^i} \tag{5.10a}$$

$$a_1(B,\tilde{B}) = \sum_{1\leq i<j\leq 3} (\frac{\tilde{\mu}}{h}[n \times \frac{B}{\mu}], \tilde{\mu}[n \times \frac{\tilde{B}}{\mu}])_{\Gamma^{ij}} + (h^{-1}[n \cdot B], [n \cdot \tilde{B}])_{\Gamma^{ij}} \tag{5.10b}$$

$$a_2(B,\tilde{B}) = (h^{-1}[n \cdot B], [n \cdot \tilde{B}])_\Gamma, \tag{5.10c}$$

$$l(\tilde{B}) = \sum_{i=1}^{3} (\mu J, \mu\nabla \times \frac{\tilde{B}}{\mu})_{\Omega^i}. \tag{5.10d}$$

If instead eliminating $B$, we would get: find $H$, such that

$$(\nabla \times H, \nabla \times \tilde{H}) + (\mu^{-1}\nabla \cdot (\mu H), \mu^{-1}\nabla \cdot (\mu\tilde{H})) \;=\; (J, \nabla \times \tilde{H}), \tag{5.11}$$

for all $\tilde{H}$. Here, we have for simplicity not included the boundary terms and the splitting into subregions.

The weighting with $\mu$ in the curl-term in the first case and with $\mu^{-1}$ in the div-term in the second, has been introduced in order to get good numerical properties. The similarity with the formulation with constant constitutive parameters is also appealing.

In a similar manner, $\tilde{\mu}$ is a suitable average that has been chosen, since $\mu$ is not defined on the interface surface. Furthermore, in the surface terms, the weight $h^{-1}$, where $h$ denotes the local mesh size, has been used in order to get correct scaling of the boundary terms, see section 3.1.3.

As mentioned above, $\alpha_1 = \alpha_2 = 10$ was chosen by numerical experiments.

It proved to be necessary to use the formulation (5.9), expressing the unknown as the flux density $B$, to achieve the correct solution. In the formulation (5.11), the field strength in the iron core became much to high, although converging slowly when refining the mesh. One possible cause of this problem is that the large difference in magnitude between the $H$ field

| | Linear | Quadratic | Reference |
|---|---|---|---|
| No of elements | 505 710 | 247 800 | - |
| No of nodes | 91 510 | 339 936 | - |
| No of nonzero matrix entries | 12 406 356 | 88 995 024 | - |
| $W_{air}$ (J) | $8.967 \times 10^{-7}$ | $9.081 \times 10^{-7}$ | $9.089 \times 10^{-7}$ |
| $W_{cu}$ (J) | $3.333 \times 10^{-8}$ | $3.581 \times 10^{-8}$ | $3.614 \times 10^{-8}$ |
| $W_{fe}$ (J) | $4.885 \times 10^{-10}$ | $4.802 \times 10^{-10}$ | $4.731 \times 10^{-10}$ |

Table 5.1: The computed magnetic energies for Problem 1 compared with reference values using LSFEM and piecewise quadratic polynomial elements. The reference values are from two dimensional computations done at ABB, see [7].

in the iron and in the air results in that certain terms in the least-squares functional dominates while other will be neglected. The $B$ field, however, is more homogeneous and thus seems to lead to a better formulation.

It may also be that the singularities have less influence on LSFEM in the $B$ field formulation, due to the same reason as above. However, the rapid increase in the least-squares residual that was noted in Problem 2, and believed to indicate the stronger singularities, has not been seen in the formulation in $H$; the behaviour of the residual is similar in the $H$ and $B$ formulation. We have also tried to eliminate the singularities by rounding of the end sections of the iron cylinder, but the problem persisted.

### 5.2.4 Computational Results

This problem was solved successfully to good accuracy, see Table 5.1. A field line plot is shown in Figure 5.3. In Figure 5.4 we plot the relative error in the magnetic energy as a function of the total number of elements, $N$, for quadratic polynomial basis functions. Note that the convergence in the air seems to be faster than in the other two regions. This might be due to unbalance between the terms in the least-squares functional in different regions.

Continuous linear polynomials have also been tested. The convergence is slower but, on the other hand, the memory requirements are less severe. The results for linear elements are plotted in Figure 5.5.

The adaptivity for these calculations was based on

$$\|h\nabla \cdot B\|_K^2, \tag{5.12}$$

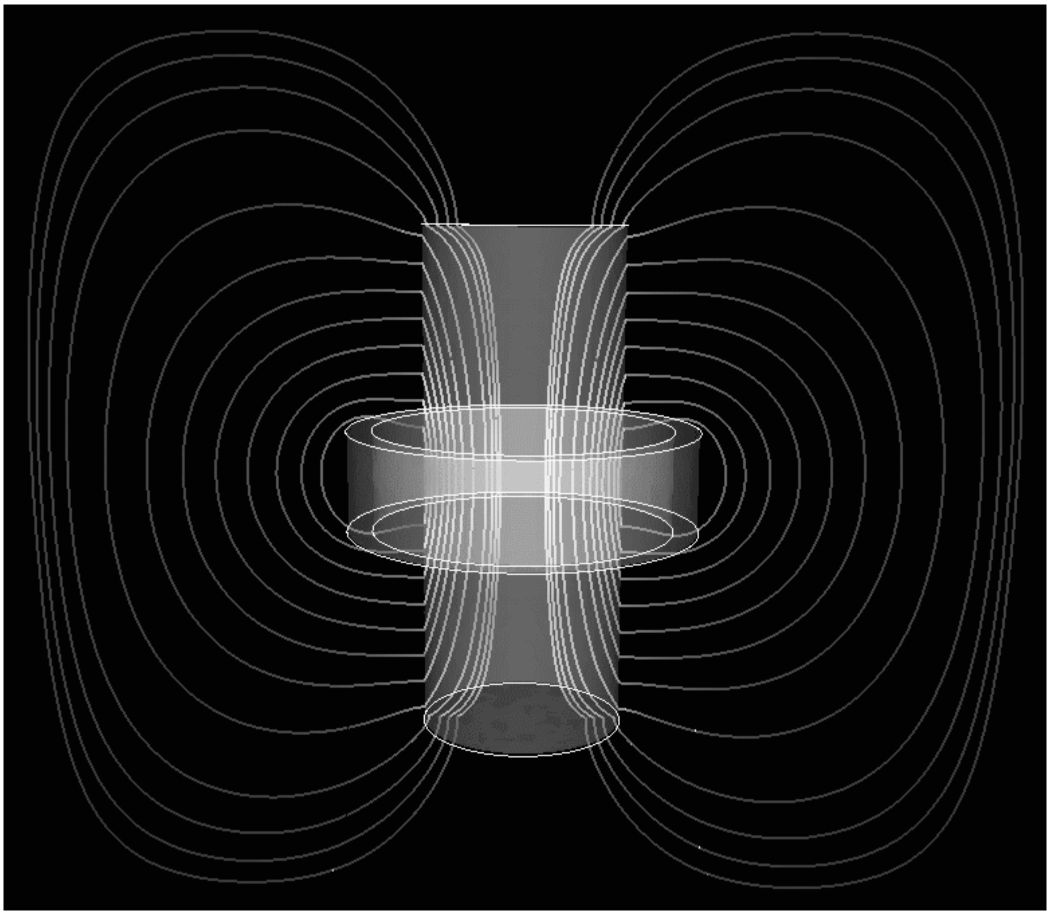

Figure 5.3: The magnetic field lines in a slice through the three dimensional solution of the axisymmetric Problem 1.

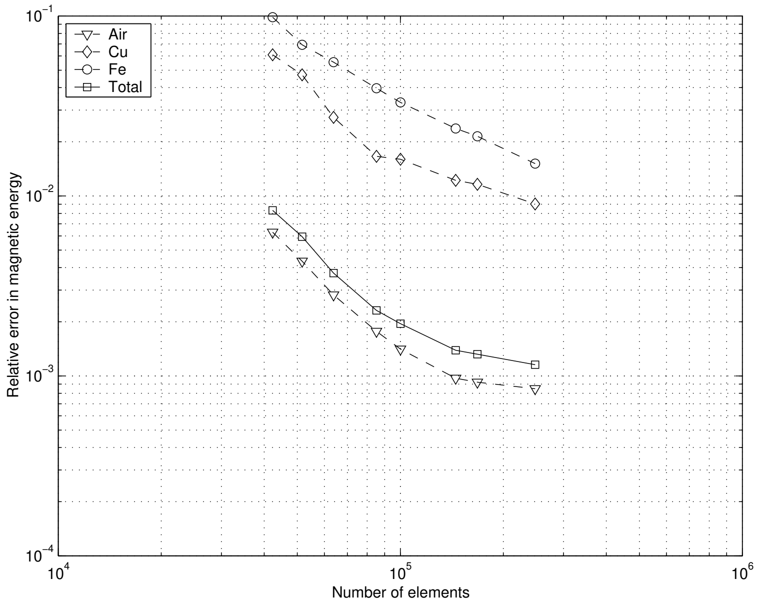


Figure 5.4: Convergence of the magnetic energy for Problem 1 using LSFEM with quadratic basis functions.

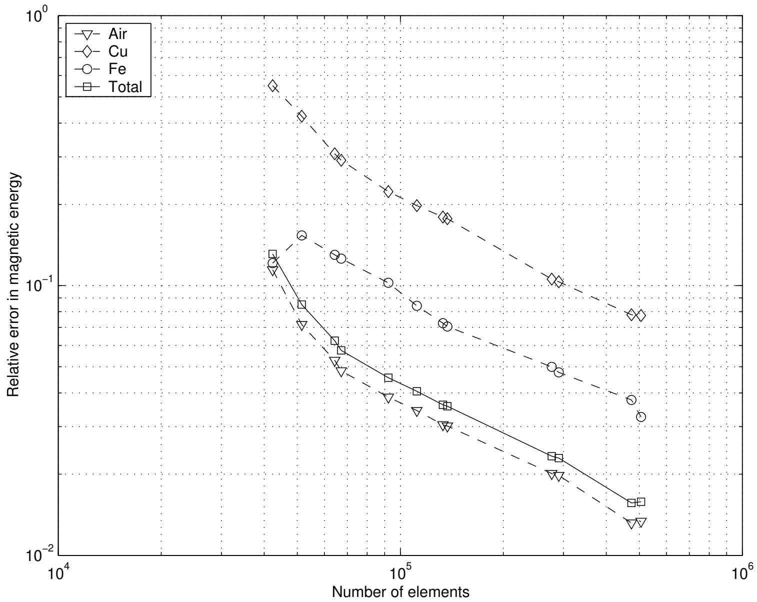


Figure 5.5: Convergence of the magnetic energy for Problem 1 using LSFEM with linear basis functions.

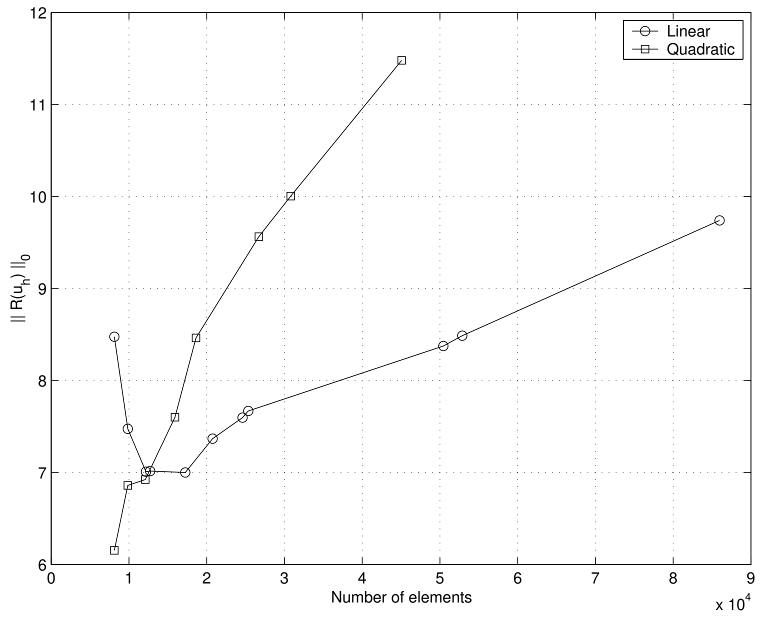


Figure 5.6: The change in the least-squares residual during grid refinement in Problem 1.

where $h$ indicates the local mesh function as mentioned above. As can be seen from Figure 5.6 the least-squares residual increases when the mesh is refined, and is thus not suitable as refinement indicator.

# 5.3 Problem 2: Another Magnetostatic Problem

## 5.3.1 Description of the Problem

The second problem is also an axisymmetric magnetostatic problem, but the geometry is slightly more complicated than in Problem 1. It is given in Figure 5.7. The copper winding is the same, but the iron part has been extended and almost encloses the coil. The data for this problem are the same as in Problem 1.

Even if this problem seems very similar to the first one, the near closure of the iron core has profound influence on the solution. Almost all of the magnetic flux will be concentrated inside the iron, while the flux density in the air is very low. This makes the singularities considerably stronger in some corners, and the larger variations in the field intensity lead to unbalance

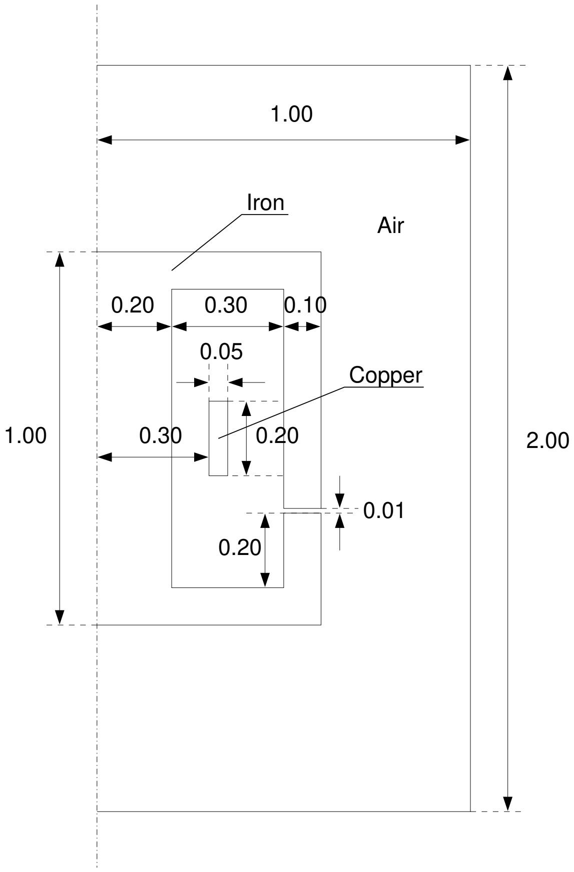


Figure 5.7: The geometry of the axisymmetric Problem 2. The dimensions are given in meters.

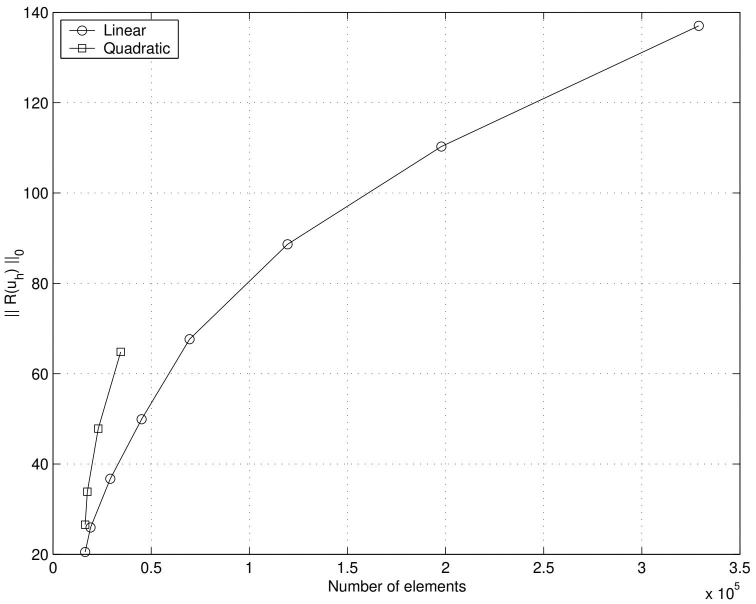


Figure 5.8: The change in the least-squares residual during grid refinement in Problem 2.

in the least-squares functional, as discussed in the previous section. In this case we do not only have the problem of differences between the materials, but also large variations between the air region enclosed by the iron and the region outside.

### 5.3.2 Results

This problem has not been successfully solved with LSFEM. The solution achieved with (5.9) have erroneous field strength inside the iron core, just as in the case when using (5.11) for Problem 1.

We can also see that the increase in the least-squares residual when refining the meshis much more dramatic in this problem than in the first one, see Figure 5.8. Since we are trying to minimize this residual, this is a strong indication of the problems in the formulation.

For a discussion on possible remedies, see Chapter 6.

## 5.4 Problem 3: A Time Harmonic Problem

### 5.4.1 Description of the Problem

As a third problem the "Asymmetrical Conductor with a Hole problem" [29], as illustrated in Figure 5.9, has been used. It consists of an aluminium plate with a hole, placed under a copper winding, modeled as a homogenous coil. There are no symmetries in this problem. The aluminium plate has a conductivity of $\sigma = 3.526 \times 10^7$ Sm$^{-1}$ and the magnetic permeability is $\mu_{r,Al} = 1$, as in the air and in the copper. Since no magnetic material is present there are no singularities as in the previuos two problems. Instead, we will get induced eddy currents in the conducting aluminium plate.

The coil is carrying a sinusoidal total current of 2742 A. The frequency is 50 Hz and the current density is constant over the cross section.

### 5.4.2 The Equations

Since the current is sinusoidal and the frequency is low, we use the quasi-static time harmonic equations

$$\nabla \times E = -j\omega B, \tag{5.13a}$$
$$\nabla \times H = J, \tag{5.13b}$$
$$\nabla \cdot B = 0, \tag{5.13c}$$

where

$$B = \mu H, \tag{5.14a}$$
$$J = J_{sc} + \sigma E. \tag{5.14b}$$

Note that Equation (5.13b) implies that $\nabla \cdot J = 0$. The interface conditions for this problem then becomes

$$[E] \times n = 0, \tag{5.15a}$$
$$[H] \times n = 0, \tag{5.15b}$$
$$[J] \cdot n = 0, \tag{5.15c}$$
$$[B] \cdot n = 0, \tag{5.15d}$$

where $n$ is a unit normal to the interface and $[\cdot]$ denotes the jump across the surface. Since $\mu_r = 1$ in the whole region, the magnetic field is continuous over surfaces. The same is true for the tangential component of the electric field, $E_t$, while (5.15c) implies that $E_{Al}^{+} \cdot n = 0$, where $E_{Al}^{+}$ denotes the field inside the aluminium plate, since $J = 0$ in the air. No further restrictions apply on the electric field.

The boundary conditions applied are

$$E \times n = 0, \tag{5.16a}$$
$$B \cdot n = 0. \tag{5.16b}$$

The placement of the outer boundary is not specified in the test case. We have enclosed the coil and the aluminium plate in a cube of approximately three times the size of a side in the plate.

### 5.4.3 The Least-Squares Formulation

Even though the magnetic field is continuous in the whole region, we still have to introduce the discontinuous elements along the surfaces, due to the jump in the normal component of $E$. Setting up the least-squares functional for this system of equations then leads to the following expression,

$$\begin{aligned} I(E,H) = \sum_{i=1}^{3} \big( & \|\nabla \times E + j\omega\mu H\|^2_{\Omega^i} \\ & + \|\nabla \times H - \sigma E - J_{sc}\|^2_{\Omega^i} + \|\nabla \cdot (\mu H)\|^2_{\Omega^i} \big) \\ & + \alpha_1 \Big( \sum_{1 \le i < j \le 3} \|[n \times E]\|^2_{\Gamma^{ij},h^{-1}} + \|n \cdot E^+\|^2_{\Gamma_{Al},h^{-1}} \Big) \\ & + \alpha_2 \sum_{1 \le i < j \le 3} \big( \|[n \times H]\|^2_{\Gamma^{ij},h^{-1}} + \|[n \cdot (\mu H)]\|^2_{\Gamma^{ij},h^{-1}} \big) \\ & + \alpha_3 \big( \|[n \times E]\|^2_{\Gamma,h^{-1}} + \|[n \cdot (\mu H)]\|^2_{\Gamma,h^{-1}} \big) \end{aligned} \tag{5.17}$$

where the second of the interface terms signify that the normal component of the $E$ field inside the aluminium should be zero on the interface.

The conditions for a minimum of $I(E, H)$ gives the following variational formulation for $U = (E, H)$: find $U$ such that

$$a_\Omega(U, \tilde{U}) + \alpha_1\, a_1(U, \tilde{U}) + \alpha_2\, a_2(U, \tilde{U}) + \alpha_3\, a_3(U, \tilde{U}) = l(\tilde{U}), \tag{5.18}$$

for all $\tilde{U}$, where

$$a_\Omega(U,\tilde{U}) = \sum_{i=1}^{3}(\nabla\times E + j\mu\omega H, \nabla\times\tilde{E} + j\omega\mu\tilde{H})_{\Omega^i} \tag{5.19a}$$
$$+ (\nabla\times H - \sigma E, \nabla\times\tilde{H} - \sigma\tilde{E}))_{\Omega^i}$$
$$+ (\nabla\cdot(\mu H), \nabla\cdot(\mu\tilde{H})))_{\Omega^i},$$
$$a_1(U,\tilde{U}) = \sum_{1\le i<j\le 3}(h^{-1}[n\times E],[n\times\tilde{E}])_{\Gamma^{ij}} \tag{5.19b}$$
$$+ (h^{-1}n\cdot E^+, n\cdot\tilde{E}^+)_{\Gamma_{Al}},$$
$$a_2(U,\tilde{U}) = \sum_{1\le i<j\le 3}(h^{-1}[n\times H],[n\times\tilde{H}])_{\Gamma^{ij}} \tag{5.19c}$$
$$+ (h^{-1}[n\cdot(\mu H)],[n\cdot(\mu\tilde{H})])_{\Gamma^{ij}}),$$
$$a_3(U,\tilde{U}) = (h^{-1}[n\times E],[n\times\tilde{E}])_{\Gamma} \tag{5.19d}$$
$$+ (h^{-1}[n\cdot(\mu H)],[n\cdot(\mu\tilde{H})])_{\Gamma}),$$
$$l(\tilde{U}) = \sum_{i=1}^{3}(J_{sc}, \nabla\times\tilde{H} - \sigma\tilde{E})_{\Omega^i}. \tag{5.19e}$$

Note that in these expressions we are dealing with complex vector fields. In practise, one separates the real and imaginary parts and thus has to work with 12 unknown variables.

### 5.4.4 Computational Results

As expected, in the absence of singularities, this problem could be solved successfully with LSFEM. Comparison with experimental data is shown in Figure 5.10. The currents induced in the aluminium plate are shown in Figure 5.11. However, due to the size of the problem, we have only been able to compute using linear polynomial basis functions and not reaching the desired accuracy. The convergence though is good as shown in Figure 5.12, since the $L^2$ norm of the residual is equivalent to the energy norm.

In this example we do not have an increasing residual, see Figure 5.12, which caused problems in the previous examples. Hence, it has also been possible to use the least-squares residual as refinement criterion:

$$I_K = \|h(\nabla\times E + j\omega\mu H)\|_K^2 \tag{5.20}$$
$$+ \|h(\nabla\times H - \sigma E - J_{sc})\|_K^2$$
$$+ \|h\nabla\cdot(\mu H)\|_K^2,$$

where $h$ indicates the local mesh function, see also section 5.1.3.

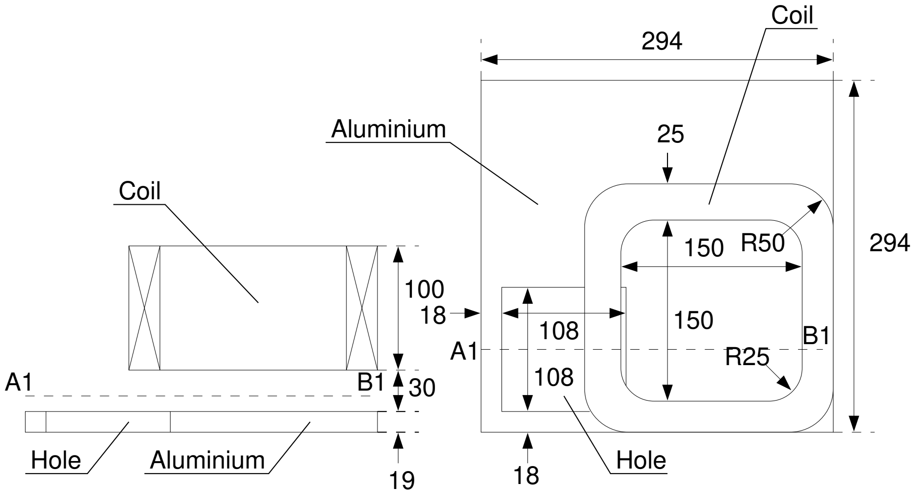


Figure 5.9: The geometry of Problem 3, a) front view, b) top view. The dimensions are given in millimeters.

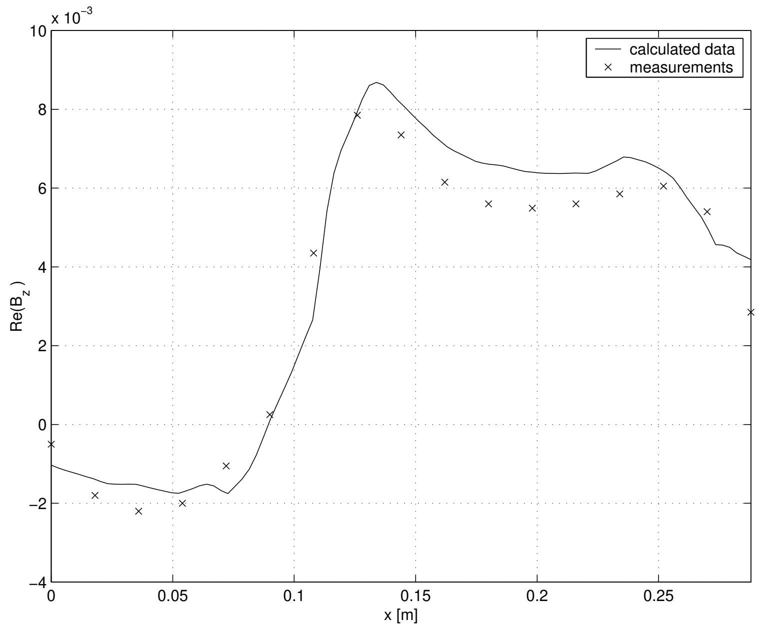


Figure 5.10: Comparison of the LSFEM solution, using linear polynomials, with experimental data for Problem 3. The values are taken along the line A1-B1 in Figure 5.9.

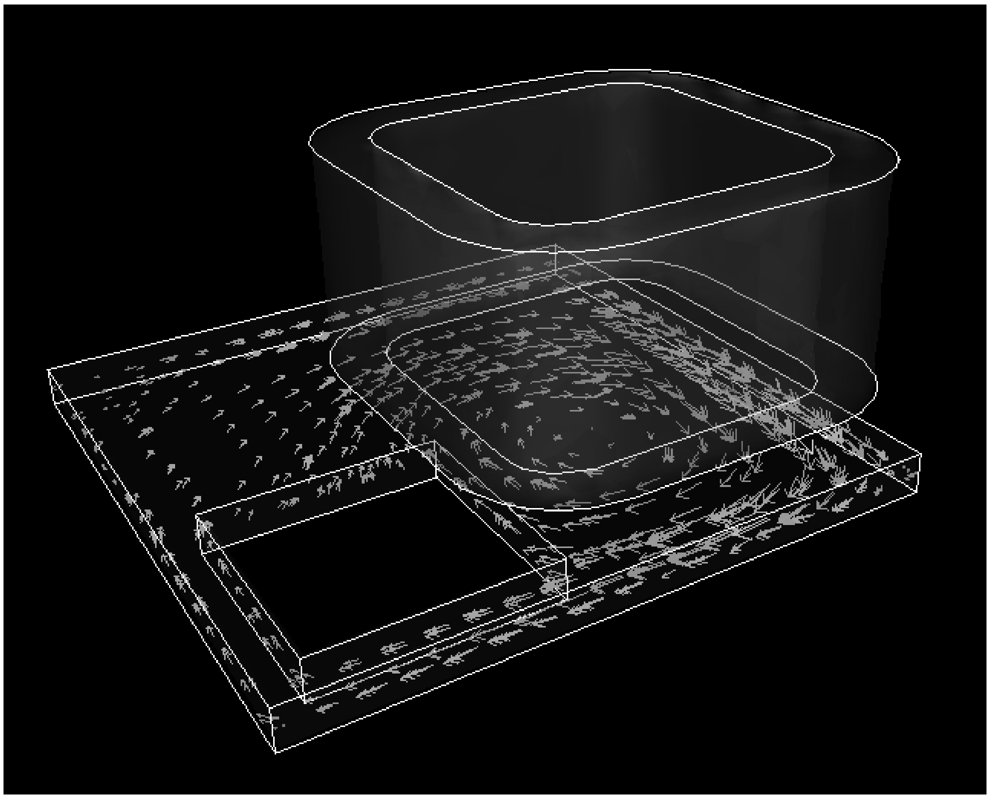

Figure 5.11: Vector plot of the induced current in the aluminium plate of Problem 3.

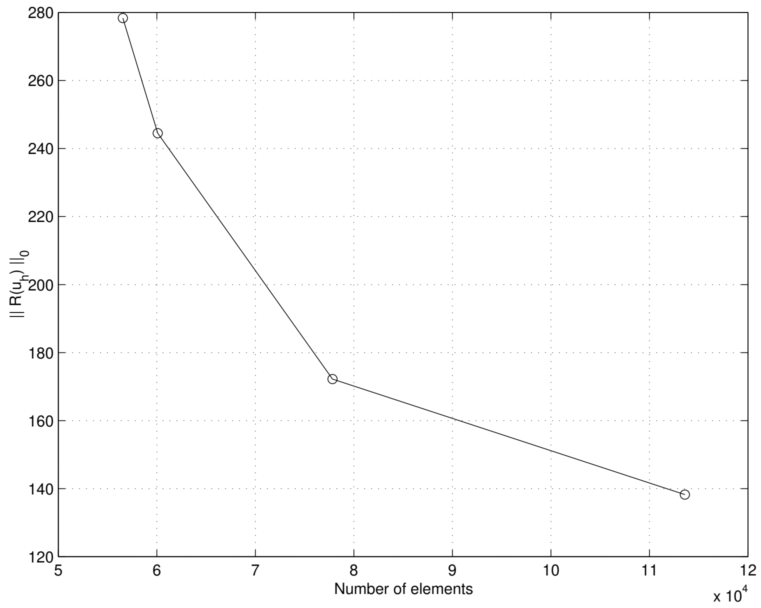


Figure 5.12: The change in the least-squares residual during grid refinement in Problem 3.

## 5.5 Numerical Dispersion Analysis

As mentioned previously, the focus of this thesis is quasi-stationary problems. In this section, we make a small exception intended to broaden the view. When dealing with wave problems, one of the important properties for a numerical method is that the dispersion error is small, i.e., the waves are travelling with the correct speed.

We have made a dispersion analysis of the Galerkin Least-Squares (GLS) finite element method, a combination of the traditional Galerkin finite element method and LSFEM, applied to the full Maxwell's equations, i.e., the low frequency approximation is not introduced. The GLS is simply formed by taking a linear combination between the standard Galerkin method and the least-squares finite element method.

One motivation for introducing the GLS method is to improve the numerical dispersion relation. The phase error in the standard Galerkin method always has the same sign, independent of the propagation direction of the wave, see for instance Monk and Parrot [24]. Here we extend the dispersion analysis to the GLS method, and as a special case, the least-squares method. We find that in the least-squares method the phase error also has the same sign independent of the direction, but with opposite sign compared with the standard Galerkin method. Further we show that by choosing the parameter in the interpolation between the standard Galerkin and the least-squares method we may improve the dispersion relation. In particular, the phase error may have different sign depending on the direction of the wave. This property is believed to be desirable for computations on unstructured grids where cancellations of phase errors with different signs may occur, see the discussion in Wu and Lee [31].

### 5.5.1 The Galerkin Least-Squares Method

For the dispersion analysis we consider the time harmonic Maxwell's equations in $\mathbf{R}^2$: find the electric and magnetic fields, $E$ and $H$, such that

$$-j\omega E - \nabla \times H = 0, \tag{5.21a}$$
$$-j\omega H + \nabla \times E = 0, \tag{5.21b}$$
$$\nabla \cdot E = 0, \tag{5.21c}$$
$$\nabla \cdot H = 0, \tag{5.21d}$$

where $\omega$ is the angular frequency.

To discretize this system of equations we introduce a subdivision of $\mathbf{R}^2$ into triangles and the corresponding finite element space $\mathcal{V}_h$ of piecewise linear continuous vector polynomials. The Galerkin least-squares (GLS) method is obtained by interpolation between the standard Galerkin method and the least-squares method and takes the form: find $U = [E, H] \in \mathcal{V}_h$, such that

$$(1-\alpha)A_G(U, \tilde{U}) + \alpha A_{LS}(U, \tilde{U}) = 0 \tag{5.22}$$

for all $\tilde{U} \in \mathcal{V}_h$, where $\alpha \in [0, 1]$ is a parameter. Further $A_G(\cdot, \cdot)$ is the bilinear form associated with the standard Galerkin method

$$A_G(U, \tilde{U}) = -(j\omega E, \tilde{E}) - (\nabla \times H, \tilde{E}) - (j\omega H, \tilde{H}) + (\nabla \times E, \tilde{H}), \tag{5.23}$$

and $A_{LS}(\cdot, \cdot)$, is the form associated with the least-squares method

$$\begin{aligned} A_{LS}(U, \tilde{U}) = (j\omega E + \nabla \times H, j\omega \tilde{E} + \nabla \times \tilde{H}) \\ + (j\omega H - \nabla \times E, j\omega \tilde{H} - \nabla \times \tilde{E}) \\ + (\nabla \cdot E, \nabla \cdot \tilde{E}) + (\nabla \cdot H, \nabla \cdot \tilde{H}). \end{aligned} \tag{5.24}$$

Note that for $\alpha = 0$ we obtain the standard Galerkin method and for $\alpha = 1$ the least-squares method. For all $\alpha \in [0, 1]$ we obtain a scheme with optimal order of convergence. The dispersion relation may however be improved by choosing the proper $\alpha$. We now turn to this topic.

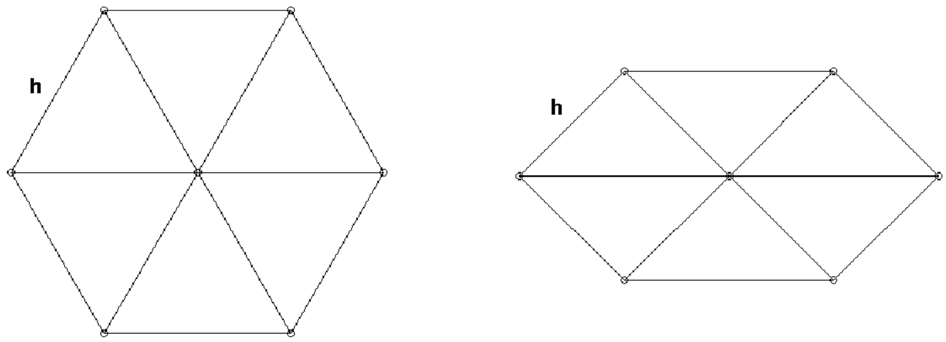


(a) *Part of an equilateral triangulation*

(b) *Part of a right angled triangulation*

Figure 5.13: The two triangulations used for the dispersion analysis.

### 5.5.2 The Dispersion Analysis

To compute the numerical dispersion, we consider a uniform triangulation of $\mathbf{R}^2$ and assume a plane wave solution propagating in the $\hat{k}$ direction ($|\hat{k}| = 1$), of the form

$$E(x) = E_0 e^{jk\hat{k}\cdot x} \qquad \text{and} \qquad H(x) = H_0 e^{jk\hat{k}\cdot x} \tag{5.25}$$

where $E_0$ and $H_0$ are constant vectors and $k$ is the wave number. For the continuous equations, this assumption yields the following dispersion relation between $\omega$ and $k$:

$$\omega = |k|, \qquad \omega = -|k|, \qquad \omega = 0, \tag{5.26}$$

independent of the direction $\hat{k}$.

If we instead insert (5.25) into the GLS finite element formulation (5.22), we get an eigenvalue problem for each node in the triangulation, which determines the numerical frequency $\tilde{\omega}$ in terms of $k$ and $\hat{k}$. Solving these eigenvalue problems for a range of $k$ and $\hat{k}$ gives the numerical dispersion relation $\tilde{\omega}(k, \hat{k})$.

Here we consider two different triangulations, one with equilateral triangles and one with right angled, see Figure 5.13. For each triangulation, we use symmetry to conclude that the eigenvalue problems associated with the nodes are identical. Thus, we obtain only one (small) eigenvalue problem for each triangulation.

### 5.5.3 Computational Results

In Figures 5.14 and 5.15 the numerical dispersion relation is plotted for the standard Galerkin and the least-squares methods respectively. The contour lines are 0.02 apart, and the quantity plotted is $|\tilde{\omega}/k|$, which should, of course, be 1. Thus the plots give an easy visual way to study the dependence of the error in the phase speed on the wavenumber $k$ and propagation direction $\hat{k}$.

We can see that for the least-squares method, the phase speed will become larger than the exact value for increasing $k$, while for the standard Galerkin method we instead get a smaller phase speed. We can also see the dependency of $\hat{k}$, which is slightly favourable for the least-squares method, at least on the equilateral triangulation.

The different behaviours of the standard Galerkin and least-squares method suggest that a properly chosen $\alpha$ in the GLS method (5.22) should produce a method with an improved dispersion relation. In Figure 5.16 we show the dispersion relation for the GLS method with $\alpha = 0.4$. This particular value of $\alpha$ is somewhat arbitrarily chosen and we plan on studying the choice of $\alpha$ in a future work.

We can see that the region $|\tilde{\omega}/k| \approx 1$ is larger for both triangulations compared with the other two methods. In particular, in Figure 5.17 we compare the regions for the standard Galerkin and least-squares methods where the phase speed error is less than 4%. In addition, for the GLS method we also obtain a phase speed that is larger than the exact value in some regions and smaller in other. This property is considered important when using unstructured triangulations, since in that case, the phase error may cancel as the wave propagates from element to element. See Wu and Lee [31] for further discussions of this topic.

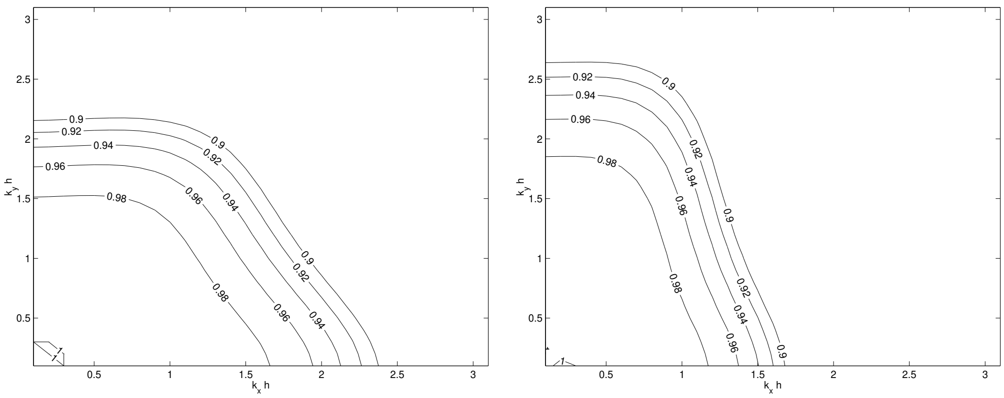


(a) *Equilateral triangulation* (b) *Right angled triangulation*

Figure 5.14: Contour maps of the phase speed error as a function of $\xi = kh\hat{k}$ for the standard Galerkin method, where $h$ is the length of the side of a triangle in the triangulation.

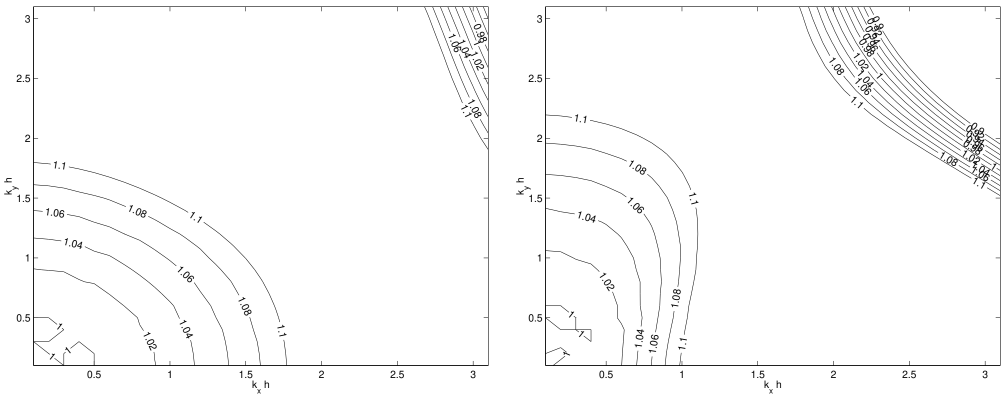


(a) *Equilateral triangulation* (b) *Right angled triangulation*

Figure 5.15: Contour maps of the phase speed error as a function of $\xi = kh\hat{k}$ for the least-squares method, where $h$ is the length of the side of a triangle in the triangulation.

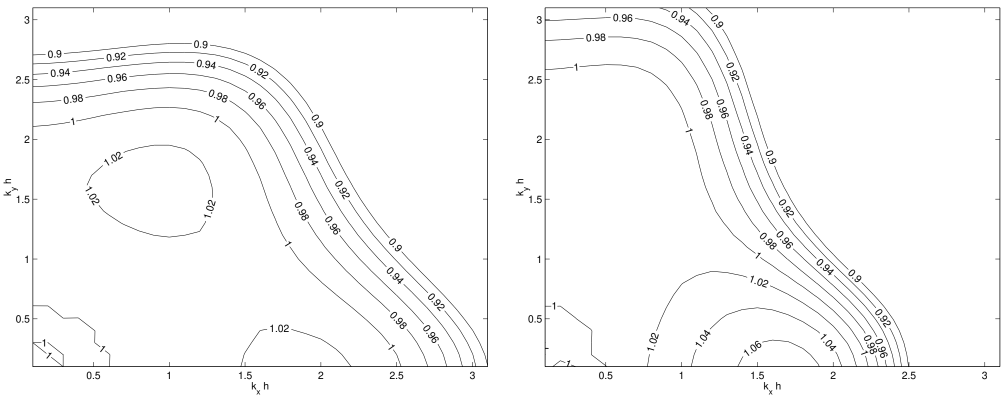


(a) *Equilateral triangulation* (b) *Right angled triangulation*

Figure 5.16: Contour maps of the phase speed error as a function of $\xi = kh\hat{k}$ for the GLS method with $\alpha = 0.4$, where $h$ is the length of the side of a triangle in the triangulation.

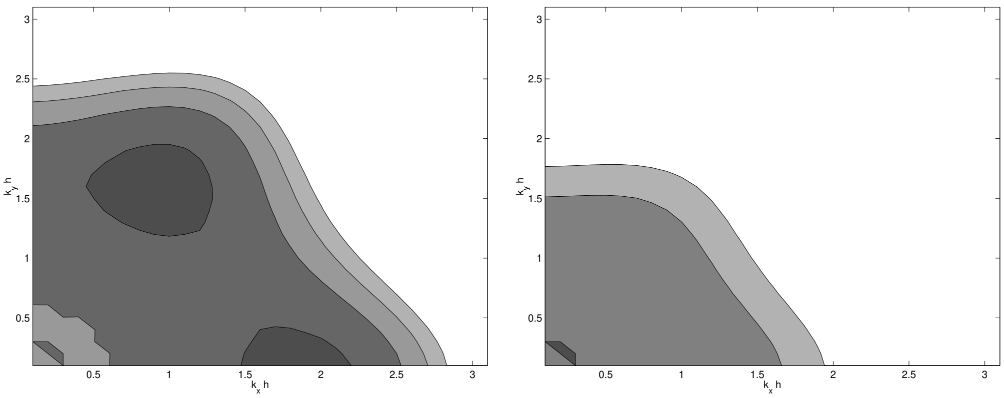


(a) *Galerkin least-squares method* (b) *Standard Galerkin method*

Figure 5.17: The coloured zone indicates the region where the phase speed error is less than 4%, for an equilateral triangulation.

# Chapter 6

# Conclusions and Future Work

## 6.1 Conclusions

The least-squares finite element method has several features that make the method suitable for electromagnetic applications. The main advantage is the natural way to include the divergence equations into the formulation and to handle the interface discontinuities. It also leads to discrete problems with good numerical properties. The possibility to formulate the problem in the primary field variables is attractive since it avoids numerical differentiation and thus leads to better accuracy and continuous fields.

In applications with realistic material parameters, we might however run into trouble with LSFEM. In three space dimensions, the grid size cannot be too small and we are not able to resolve all features in the solution. The least-squares functional might then be unbalanced, leading to unacceptably low accuracy. Some weighting of the different terms in the functional seems to be needed.

The formulation in primary variables naturally also have problems when the field is singular. Weak enforcement of boundary conditions reduces the effect of the singularity somewhat, but also here it seems to help to introduce weighted norms.

## 6.2 The Problem with Correct Weights

In these applications, the large material parameters seem to cause unbalance in the least-squares problem. The way to handle this unbalance has been to use weighted norms with carefully chosen weights. In Problem 1, we solved for the $B$ field with the curl term multiplied by $\mu$. For the third problem, we instead formulated the functional in the $H$ field without weights.

However, as could be seen in Problem 2, these weights might not be easy to establish, thus making the problem difficult to solve. One approach to automatically compute appropriate weights could be to introduce a dual problem. It is possible to tailor an a posteriori error indicator to a specific quantity in a problem using the dual problem, see Rannacher [26]. This leads to an indicator expressed as a weighted sum of the residuals, where the solution to the dual problem gives the weights. In a similar fashion, a weighted least-squares functional could possibly be formed based on the solution of a dual problem.

## 6.3 How to Deal with Singularities

In regions where the solution is smooth, the least-squares approach works very well. But, as can be seen from Theorem 3.1.3, it requires more regularity than standard Galerkin. In fact, the solution must belong to $H^{r+1}$, where $r > 0$, in order to have guaranteed convergence. This is often not the case, e.g. when the domain have corners or edges. It has also been observed that mesh refinement alone cannot resolve the suboptimal convergence [22].

This problem has attracted some attention in the case of the div-grad problem [12]. The remedy proposed was to use a weighted $L^2$ norm, $\| \cdot \|_{r^\beta}$, where $r$ is the distance to the singularity and $\beta$ depends on the strength of the singularity.

In practical computations, this kind of weighting function is very cumbersome, if even possible, to compute. First, one has to locate the singularity, and then compute the correct weight $\beta$. This should preferably be done without prior knowledge of the geometry or the solution.

## 6.4 The $H^{-1}$ Approach

An idea in LSFEM is to use weaker norms, such as the $H^{-1}$ norms, when forming the least-squares functional, rather than the more practical $L^2$ norms. The concept of using a weaker norm was already discussed in the previuos section when introducing a weight to eliminate the singularities, and also, the way to use the $H^{-1}$ norm is similar to using the dual problem to calculate the weights as desribed in section 6.2.

The space $H^{-1}$ is the dual space to the Sobolev space $H^1$, and the norm is defined by

$$\|v\|_{-1}^2 = sup_{\phi \in H_0^1} \frac{(v, \phi)}{\|\phi\|^2}. \tag{6.1}$$

This norm, and the corresponding inner product, can be computed as

$$\|v\|_{-1}^2 = (Tv, v), \tag{6.2}$$

where $T$ is the solution operator to a Poisson type problem, see Bramble, Lazarov, and Pasciak [9]. Furthermore, it is possible to replace $T$ by a computable operator $T_h$, constructed via a preconditioner to the defining Poisson type problem, leading to the discrete equivalent $H^{-1}$ norm,

$$\|v\|_{-1,h}^2 = (T_h v, v). \tag{6.3}$$

The $H^{-1}$ least-squares approach allows for less smooth data and solutions, compared with using $L^2$ norms. It may however be more sensitive to unbalanced terms in the least-squares functional, but a correctly formed operator $T_h$, taking the underlying equations into account, should be able to circumvent this problem.

# Bibliography

[1] First-order system least squares philosophy. ftp://amath.colorado.edu/pub/fosls.

[2] F. Assous, P. Ciarlet, and E. Sonnendrücker. Resolution of the Maxwell equations in a domain with reentrant corners. *Modél. Math. Anal. Numér.*, 32(3):359–389, 1998.

[3] F. Assous, P. Degond, E. Heintze, P.A. Raviart, and J. Segre. On a finite-element method for solving the three-dimensional Maxwell equations. *J. Comp. Phys*, 109:222–237, 1993.

[4] S. Balay, W.D. Gropp, L.C. McInnes, and B.F. Smith. Efficient management of parallelism in object oriented numerical software libraries. In E. Arge, A. M. Bruaset, and H. P. Langtangen, editors, *Modern Software Tools in Scientific Computing*, pages 163–202. Birkhauser Press, 1997.

[5] S. Balay, W.D. Gropp, L.C. McInnes, and B.F. Smith. PETSc 2.0 users manual. Technical Report ANL-95/11 - Revision 2.0.28, Argonne National Laboratory, 2000.

[6] S. Balay, W.D. Gropp, L.C. McInnes, and B.F. Smith. PETSc home page. http://www.mcs.anl.gov/petsc, 2000.

[7] R. Bergström, A. Bondeson, C. Johnson, M.G. Larson, Y. Liu, and K. Samuelsson. Adaptive finite element methods in electromagnetics. Technical Report 2, Swedish Institute of Applied Mathematics (ITM), 1999.

[8] P.B. Bochev and M.D. Gunzburger. Finite element methods of least-squares type. *SIAM Rev.*, 40(4):789–837, 1998.

[9] J.H. Bramble, R.D. Lazarov, and J.E. Pasciak. A least-squares approach based on a discrete minus one inner product for first order systems. *Math. Comp.*, 66:935–955, 1997.

[10] S.C. Brenner and L.R. Scott. *The Mathematical Theory of Finite Element Methods.* Springer-Verlag, 1994.

[11] M. Costabel and M. Dauge. Singularities of Maxwell's equations on polyhedral domains. In *Analysis, numerics and applications of differential and integral equations*, number 379 in Pitman Res. Notes Math. Ser., pages 69–76. Longman, Harlow, 1998.

[12] C.L. Cox and G.J. Fix. On the accuaracy of least squares methods in the presence of corner singularities. *Comp. & Maths. with Appls.*, 10(6):463–475, 1984.

[13] K. Eriksson, D. Estep, P. Hansbo, and C. Johnson. *Computational Differential Equations.* Cambridge University Press, 1996.

[14] L.C. Evans. *Partial Differential Equations.* American Mathematical Society, 1998.

[15] V. Girault and P.A. Raviart. *Finite Element Methods for Navier-Stokes Equations.* Springer-Verlag, 1986.

[16] J. Ivarsson. A posteriori error analysis of a finite element method for the time-dependent Ginzburg-Landau equations. Preprint 24, Department of Mathematics, Chalmers University of Technology, 1998.

[17] D. Jespersen. A least-squares decomposition method for solving elliptic equations. *Math. Comp.*, 31:873–880, 1977.

[18] B.-N. Jiang. *Least-squares finite element method : Theory and applications in computational fluid dynamics and electromagnetics.* Springer-Verlag, 1998.

[19] B.-N. Jiang, J. Wu, and L.A. Povinelli. The origin of spurious solutions in computational electromagnetics. *J. Comp. Phys.*, 125:104–123, 1996.

[20] X. Jiao, X.Y. Li, and X. Ma. SIFFEA: Scalable integrated framework for finite element analysis. In S. Matsuoka, R.R. Oldehoeft, and M. Tholburn, editors, *Computing in Object-Oriented Parallel Environments*, pages 84–95, 1999.

[21] H.P. Langtangen. *Computational Partial Differential Equations.* Springer-Verlag, 1999.

[22] Y. Lee. *Shear Bands in Elastic-Perfectly Plastic Media.* PhD thesis, Carnegie-Mellon University, 1981.

[23] T.A. Manteuffel, S.F. McCormick, and C. Pflaum. Improved discretization error estimates for first-order system least squares (FOSLS). ftp://amath.colorado.edu/pub/fosls, Submitted.

[24] P.B. Monk and A.K. Parrot. A dispersion analysis of finite element methods for Maxwell's equations. *SIAM J. Sci. Comp.*, 15(4):916–937, 1994.

[25] A.I. Pehlivanov, G.F. Carey, and P.S. Vassilevski. Least-squares mixed finite element methods for non-selfadjoint problems: I. error estimates. *Numer. Math.*, 72:501–522, 1996.

[26] R. Rannacher. A posteriori error estimation in least-squares stabilized finite element schemes. *Comp. Methods Appl. Mech. Engrg.*, 166:99–114, 1998.

[27] L.R. Scott and S. Zhang. Finite element interpolation of nonsmooth functions satisfying bundary conditions. *Math. Comp.*, 54:483–493, 1990.

[28] M. Touma Holmberg. *Three-dimensional Finite Element Computation of Eddy Currents in Synchronous Machines.* PhD thesis, Dept. of Electric Power Engineering, Chalmers University of Technology, 1998.

[29] L. Turner. Benchmark problems for the validation of eddy current computer codes. *COMPEL*, 9:123–216, 1990.

[30] W. Wendland. *Elliptic Systems in the Plane.* Pitman, 1979.

[31] J.Y. Wu and R. Lee. The advantages of triangular and tetrahedral edge elements for electromagnetic modeling with the finite-element method. *IEEE Trans. Antennas Propagat.*, 45(9), 1997.

# Chalmers Finite Element Center Preprints

1999–001 *On Dynamic Computational Subgrid Modeling*

Johan Hoffman and Claes Johnson

2000–001 *Adaptive Finite Element Methods for the Unsteady Maxwell's Equations*

Johan Hoffman

2000–002 *A Multi-Adaptive ODE-Solver*

Anders Logg

2000–003 *Multi-Adaptive Error Control for ODEs*

Anders Logg

2000–004 *Dynamic Computational Subgrid Modeling* (Licentiate Thesis)

Johan Hoffman

These preprints can be obtained from

**www.phi.chalmers.se/preprints**